RESEARCH

Experimental Evaluation of Effect Factors on Seismic Performance of Concrete Columns Reinforced with HTRB630 High-Strength Steel Bars

Chuanzhi Sun[1], Mei-Ling Zhuang[2,3]* and Bo Dong[4]

Abstract

HTRB630 steel bar is a new type of high-strength steel bars. To study the seismic performance and promote the application of concrete columns reinforced with HTRB630 high-strength steel bars, the pseudo-static test of 10 concrete columns reinforced with HTRB630 high-strength steel bars and 3 concrete columns reinforced with HRB400 was carried out. Test specimens were divided into five categories according to concrete grade, reinforcement strength, and degree of confinement. The effect of concrete strength (C45 and C60), axial load ratio (0.1 and 0.25), equal strength substitution of longitudinal reinforcements (HTRB630 and HRB400), equal strength and volume substitution of stirrups (HTRB630 and HRB400), equal strength substitution of confined reinforcements (HTRB630 and HRB400) on the seismic performance are analyzed and discussed from the failure mode, hysteresis loops, skeleton curves, lateral strength, ductility, energy dissipation capacity, stiffness and strength degradation. The failure mode of each specimen was bending failure. Reducing of the axial lo ratio or increasing the strength of reinforcements, the seismic performance of the specimen could be improved. C60 concrete can improve the seismic performance of HTRB630 reinforced columns. The lateral strength of the concrete column specimen with HTRB630 reinforcements was slightly increased, and the ductility and energy dissipation capacity were reduced, the stiffness degradation was more gradual, the strength degradation coefficient was greater than 0.94, but still met the requirements of the code for seismic design of buildings (GB50011-2010).

Keywords: HTRB630 high-strength steel bars, seismic performance, failure modes, hysteretic loops, skeleton curves, bear capacity and ductility, energy dissipation capacity, stiffness degradation

1 Introduction

Reinforced concrete (RC) structures have the advantages of lower cost, higher stiffness and better sound insulation than steel structures. Therefore, the research and application of high-strength reinforcing steel (reinforcements with yield strength of 400 MPa and above) are important in many countries (Lai et al., 2019). At present, in Europe and the United States, 400 and 500 MPa steel bars have become the main reinforcing steel bars. The proportion of high-strength steel bars with strength of 400 to 630 MPa has reached more than 95%. ACI 318–08 code (Committee, 2008) stipulated that the maximum yield strength of common longitudinal steel reinforcements was 550 MPa. European standard specification (BS Eurocode, 2004) allowed the maximum yield strength of common longitudinal steel reinforcements to be 630 MPa.

*Correspondence: ml_zhuang99@163.com

[2] School of Transportation and Civil Engineering, Nantong University, Jiangsu Province 226019 Nantong, China
Full list of author information is available at the end of the article

Sun *et al. Int J Concr Struct Mater*   (2022) 16:45

Page 2 of 28

Columns are one of the main load-bearing members of concrete structures. The seismic performance of columns has a great impact on the performance of the structure under earthquakes. Many scholars in China have conducted experiment on the seismic performance of concrete columns with high-strength reinforcements (Liu et al., 2014; Su et al., 2014; Wang et al., 2013, 2015), but most of the steel bar strength of test specimens is 500 MPa and below. In recent years, there have been more and more varieties of steel bars with strength higher than 500 MPa in China, and they have also been applied in actual projects. However, there are few studies on the 630 MPa-grade steel bars. HTRB630E steel bar is a new type of high-strength steel bar independently developed and produced by Jiangsu Tianshun Material Group Co., Ltd, China. The standard value of its yield strength has reached over 630 MPa, and the standard value of ultimate strength has exceeded 790Mpa (T63 Heat Treatment Technical Specification for Ribbed High Strength Reinforced Concrete Structure: Q3, 21182 KBC001-2016. 2016). The difference between HTRB630 steel bars and low-strength hot-rolled steel bars mainly includes two aspects as follows. (1) nickel, chromium, vanadium, etc. are added in HTRB630E steel bars during production. Trace elements, through the precipitation of carbides and nitrides of these trace elements in steel, achieve the purpose of grain refinement and precipitation strengthening. (2) The cooling process of HTRB630E steel bars is different from low-strength hot-rolled steel bars. The low-strength hot-rolled steel bars use "natural cooling in the air", while the 630 MPa ultra-high-strength steel bars use "temperature-controlled cooling". The crystal structure of the core is consistent, and both the edge and the core are composed of ferrite and pearlite (Sun et al., 2021).

The columns reinforced with high-strength steel bars can offer many advantages, such as reducing the required amount of reinforcing steel, avoiding the congestion of reinforcing bars, improving the casting quality of concrete, simplifying the design and construction of joints and members. To promote the application of high strength steel in RC structures, there have been extensive research works on concrete members reinforced with high-strength steel bars. Zhang et al. (2015) conducted quasi-static tests on bridge piers with 500 MPa high-strength steel bars, and analyzed the effects of axial load ratio, shear-span ratio, stirrup spacing and reinforcement strength on hysteretic loops, strength, ductility and energy dissipation of specimens. Su et al. (2014) conducted quasi-static tests on 10 concrete columns reinforced with different reinforcements (HRB335, HRB500E, HRB600). It found that the strength and ductility of specimens changed greatly when the reinforcement was replaced with equal volume;

the seismic performance of the specimen changed little when the steel bar was replaced with equal strength. Aoyama (1992) compared the pseudo-static test results of concrete columns with longitudinal reinforcements of 400 MPa and 700 MPa. Ousalem (2009) carried out low-cycle cyclic test on 1/4-scale concrete columns reinforced with 685 MPa and 980 MPa steel bars, which indicated that the columns reinforced with 980 MPa steel bars have better ductility and less residual deformation. Rautenberg (2012) proved through experiments that the reduction of the reinforcement area will not significantly reduce the lateral strength and displacement ductility of specimens with sufficient transverse reinforcements. Based on the above research, it can be concluded that: (1) there are few studies on concrete rectangular columns reinforced with HTRB630 high-strength steel bars; (2) the concrete columns reinforced with high-strength steel bars have good lateral strength and ductility, although their ductility is not as good as those with common steel bars; (3) the main effect factors on the seismic performance of columns reinforced high-strength steel bars are concrete strength, axial load ratio, equal strength substitution of reinforcements etc.

To improve the brittleness of high-strength concrete, confined concrete is often used in engineering. Many scholars have studied the concrete structure confined by high-strength stirrups, but few of them are HTRB630 steel reinforcements. Sun et al. (2010) calculated the pseudo-static test data of 98 rectangular concrete columns with high-strength stirrups and 11 circular concrete columns with high-strength stirrups. The result indicated that the main factor affecting the displacement ductility and seismic performance of high-strength reinforced concrete columns is the characteristic value of the hoop, axial load ratio, longitudinal reinforcements, and thickness of concrete cover. Muguruma et al. (1990) carried out low-cycle repeated tests on 8 high-strength concrete column specimens. The results indicated that the ductility of high-strength concrete columns can be improved obviously with high-strength stirrups. Sugano et al. (1990) studied the seismic performance of high strength concrete columns with high-strength stirrups to prove that the high-strength reinforcements and high-strength concrete can effectively improve the strength and ductility of reinforced concrete members. Bayrak et al. (1997) completed low-cycle repeated tests on 7 concrete columns. The concrete grade range of test specimens was 30~70 MPa, and the stirrup strength range was 440~540 MPa. Test results indicated that high-strength concrete columns with an appropriate number and reasonable ratio of high-strength stirrups, the ductility coefficient of high-strength concrete columns can be increased to 7.0. Budek et al. (2002) conducted a

Sun *et al. Int J Concr Struct Mater*   (2022) 16:45

Page 3 of 28

pseudo-static test on 9 pier columns using pre-stressed steel wires (1570 MPa) as the transverse reinforcements. The results indicated that the high-strength spiral stirrup effectively delays the buckling of the longitudinal reinforcements. Whether the final failure mode was bending failure or shear failure, the ductility of specimens could meet the requirements. Based on the above research, it can be concluded that: (1) reasonable allocation of high-strength stirrups can effectively improve the ductility of high-strength concrete, and dense allocation of high-strength stirrups is an effective method to improve the limit value of axial load ratio of high-strength concrete columns; (2) axial load ratio and stirrup ratio have obvious effects on the seismic performance of concrete columns; (3) increasing stirrup strength is not as good as increasing stirrup ratio, which has a great impact on the ductility of concrete columns.

To study the seismic performance and promote the application of concrete columns reinforced with HTRB630 high-strength steel bars, the pseudo-static test of 10 concrete columns reinforced with HTRB630 high-strength steel bars and 3 concrete columns reinforced with HRB400 was carried out. The effect of concrete strength, axial load ratio, equal strength substitution of longitudinal reinforcements, equal strength and volume substitution of stirrups, equal strength substitution of confined reinforcements on the seismic performance are analyzed and discussed from the failure mode, hysteresis loops, skeleton curves, ductility, energy dissipation capacity and stiffness. The article was organized as follows. In Sect. 2, experimental program was introduced. In Sect. 3, test results and analysis were given. In Sect. 4, analysis of effect factors on the seismic performance of specimens were analyzed and discussed. Finally, conclusions and suggestions were presented in Sect. 5.

2 Experimental Program

2.1 Test Objectives

The use of HTRB630 high-strength steel bars has obvious economic advantages. The first purpose of the experiment was to study the seismic performance of concrete columns reinforced with HTRB630 high-strength reinforcements and HRB400 reinforcements. For this purpose, specimens numbered $1 \sim 11$ were designed and tested under the pseudo-static loads.

At present, the main idea of improving the ductility of high-strength concrete is to provide effective lateral confinement. To study the confining effect of HTRB630 high-strength stirrups on high-strength concrete, the specimens numbered 12 (concrete columns with HRB400 high-strength stirrups) and 13 (concrete columns with HTRB630 high-strength stirrups) were designed and tested. Compared with the previous 11 specimens, the

spacing of stirrups was greatly reduced, and the confined efficiency was also greatly increased. The purpose of designing this group of specimens was to verify the effectiveness of high-strength confined stirrups.

2.2 Design of Specimens

To investigate the effect factors on the seismic performance of concrete columns reinforced with HTRB630 high-strength steel bars, 10 concrete columns reinforced with HTRB630 high-strength steel bars and 3 concrete columns reinforced with HRB400 were designed according to concrete strength (C45 and C60), axial load ratio (0.1 and 0.25), equal strength substitution of longitudinal reinforcements (HTRB630 and HRB400), equal strength and volume substitution of stirrups (HTRB630 and HRB400), equal strength substitution of confined reinforcements (HTRB630 and HRB400). The specimens were composed of the lower base and the upper concrete column, which were cast in situ as a whole and formed at one time. The base was a cuboid of 1350 mm × 550 mm × 700 mm, the thickness of concrete cover concrete was 50 mm, and the steel reinforcement were all HRB400 (C) reinforcements. The upper concrete column had a section size of 250 mm × 250 mm, symmetrical reinforcement, a cover concrete thickness of 20 mm. The bottom of the longitudinal bar was bent 90° to ensure sufficient anchoring length (350 mm). It was bound and fixed with the bottom steel bars of the base. The C 10 @ 50 stirrups were uniformly arranged within the 300 mm height of column top. The design value of the yield strength f_y was taken as the reinforcement strength according to the code (GB50010-2010) (MOHURD, 2015). The design value of the yield strength of HRB400 steel bars was f_y, 400 = 360 MPa in MOHURD (2015). There was no ready-made national specification for HTRB630 steel bars, according to technical specification (JG/T 054-2012) (2012) in Jiangsu Province for heat treatment of ribbed high-strength reinforced concrete structure, the design value of the yield strength of HTRB630 steel bars was f_y, 630 = 525 MPa. The details of specimens are shown in Fig. 1 and photo of some specimens is shown in Fig. 2. HTRB630 steel bars are indicated by the symbol D. The design parameters of 13 specimens are shown in Table 1. In Table 1, "H45-1″ represents the first C45 concrete columns reinforced with HRB400 longitudinal reinforcements; "T60-1″ represents the first C60 concrete columns reinforced with HTRB630 longitudinal reinforcements; A_s represents the strength, number and diameter of the longitudinal steel reinforcements; $A_{s,v}$ represents the strength, number and diameter of stirrups.

According to concrete grade, reinforcement strength and degree of confinement stirrups, the reinforced

Sun *et al. Int J Concr Struct Mater*   (2022) 16:45

Page 4 of 28

Fig. 1 Details of specimens (unit: mm).

Fig. 2 Photo of some specimens.
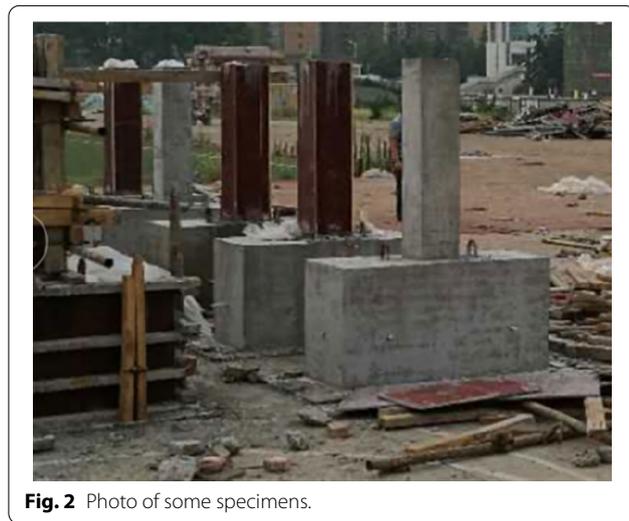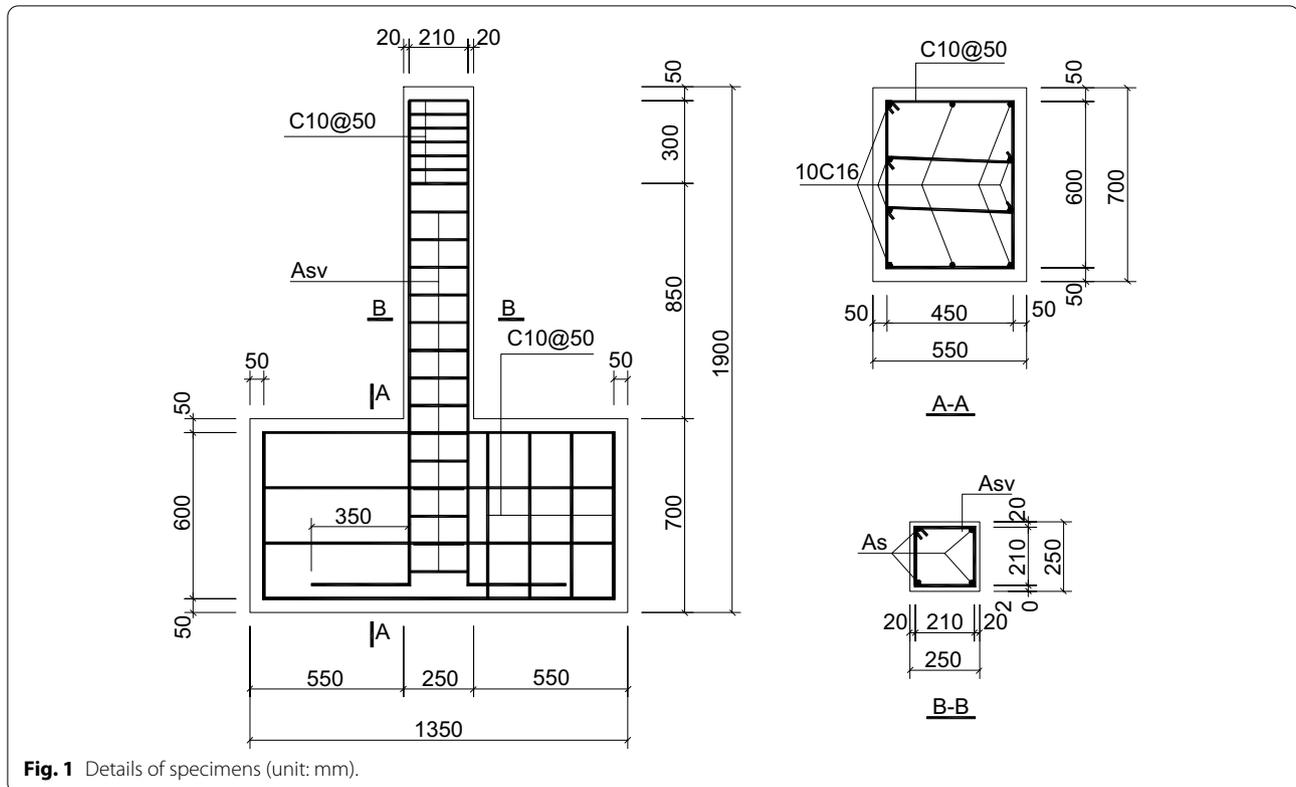
concrete columns in Table 1 can be roughly divided into five categories as follows.

(1) Common concrete columns with common reinforcements (CCC-CRs): H45-1, H45-2.
(2) Common concrete columns with high-strength reinforcements (CCC-HRs): T45-1, T45-2, T45-3, T45-4, T45-5.

(3) High-strength concrete columns with common reinforcements (HCC-CRs): H60-1.
(4) High-strength concrete columns with high-strength reinforcements (HCC-HRs): T60-1, T60-2, T60-3.
(5) Confined high strength concrete columns (CHCCs): T60-4, T60-5.

The reinforced concrete columns could be roughly divided into six groups to analyze the factors on the seismic performance of specimens according to axial load ratio (I), grade of concrete (II), equal strength substitution of longitudinal reinforcements (III), equal strength substitution of stirrups (IV), equal volume substitution of stirrups (V), equal strength substitution of confined stirrups (VI), as shown in Table 2.

2.3 Mechanical Properties of Concrete and Steel Bars

Concrete C45 and C60 were used for the fabrication of test specimens. Three concrete cubes with 150 mm side length were reserved for the two grades, which were manufactured at the same time and cured under the same conditions as the test specimens. Three steel bar specimens of HRB400 and HTRB 630 were also taken for the test. The mechanical properties of concrete and steel were tested according to the material test standard (MOHURD, 2012, 2015; National standards of People's

Sun *et al. Int J Concr Struct Mater*   (2022) 16:45

Page 5 of 28

Table 1 Parameters of specimens.

Specimen		Concrete grade	Axial load ratio n	Axial force N (kN)	Shear-span λ	A_s	Longitudinal reinforcement ratio ρ (%)	A_{sv}	Stirrup ratio $ρ_{sv}$ (%)
Number	Name								
1	T45-1	C45	0.10	201	5.58	4D14	0.985	C8@100(2)	1.100
2	T60-1	C60	0.25	641	5.58	4D14	0.985	C8@100(2)	1.100
3	T45-2	C45	0.25	502	5.58	4D14	0.985	C8@100(2)	1.100
4	H45-1	C45	0.10	201	5.63	4C18	1.630	C8@100(2)	1.160
5	H45-2	C45	0.25	502	5.63	4C18	1.630	C8@100(2)	1.160
6	H60-1	C60	0.25	641	5.63	4C18	1.630	C8@100(2)	1.160
7	T45-3	C45	0.10	201	5.58	4D14	0.985	D8@150(2)	0.736
8	T45-4	C45	0.25	502	5.58	4D14	0.985	D8@150(2)	0.736
9	T60-2	C60	0.25	641	5.58	4D14	0.985	D8@150(2)	0.736
10	T45-5	C45	0.25	502	5.58	4D14	0.985	D8@100(2)	1.100
11	T60-3	C60	0.25	641	5.58	4D14	0.985	D8@100(2)	1.100
12	T60-4	C60	0.25	641	5.58	4D14	0.985	C8@50(2)	2.210
13	T60-5	C60	0.25	641	5.58	4D14	0.985	D8@75(2)	1.470

Table 2 Group classification.

Group	Specimens
I	(H45-1, H45-2), (T45-3,T45-4)
II	(T60-1,T45-2), (H45-2,H60-1), (T45-4,T60-2), (T45-5,T60-3)
III	(T45-2,H45-2), (T60-1,H60-1)
IV	(T45-2,T45-4), (T60-1,T60-2)
V	(T45-2,T45-5), (T60-1,T60-3)
VI	(T60-4,T60-5)

Republic of China, 2010) as shown in Tables 3 and 4. In Table 3, $f_{cu,0}$ was the average value of measured cube compressive strength; $f_{cu,k}$ was the standard value of cube compressive strength; f_{ck} was the standard value of axial compressive strength of concrete; f_{tk} was the standard value of axial tensile strength; E_c was the elastic modulus of concrete. The measured stress–strain ($σ–ε$) curves of specimens are shown in Fig. 3.

From Table 3 and Fig. 3, it could be seen that:

Table 3 Test and calculation results of concrete.

Grade	Cube compressive strength (MPa)		$f_{cu,k}$	Concrete mechanical index		
	$f_{cu,0}$	Σ		f_{ck}(MPa)	f_{tk}(MPa)	$E_c(× 10^4$ MPa)
C45	52.9	2.5	48.8(C45)	32.1	2.80	3.43
C60	66.9	1.9	63.8(C60)	41.0	3.13	3.64

Table 4 Test results of reinforcements.

Mechanical properties	HRB400(C)	HTRB630(D)
Yield strength bottom limit f_y'(MPa)	453.44	738.34
Yield starting point strain $ε_y$ ($× 10^{-3}$)	2.302	3.355
Elastic modulus E_s (GPa)	190.34	219.08
Starting point strain of strain hardening section $ε_{sh}$ ($× 10^{-3}$)	25.27	12.38
Initial modulus of strain hardening section E_{sh} (MPa)	5.61	9.59
Ultimate strength f_u (MPa)	614.76	928.50
Strain at strength limit point $ε_{ult}$ ($× 10^{-3}$)	144.44	89.64

Fig. 3 Stress–strain (σ–ε) curves of reinforced specimens.
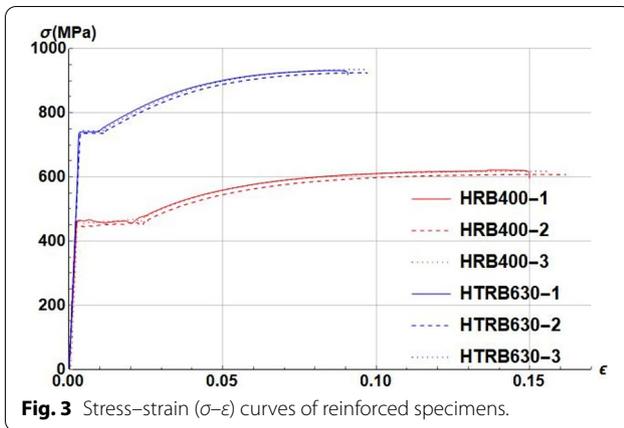
(1) The yield strength of HRB400 and HTRB630 steel bars was greater than the specification requirement in Jiangsu Tianshun Metal Materials Group Co., Ltd., And School of Civil Engineering in Southeast University (2012). The mechanical properties of the steel bars met the standard. The measured mechanical properties of two reinforced specimens with the same strength were relatively close, indicating that the reliability of specimens was better.

(2) The stress–strain curves of HTRB630 high-strength steel bars had also undergone four stages: elasticity, yielding, strengthen*i*ng, and necking. Compared with HRB400 steel bars, HTRB630 steel bars had higher yield strength and the starting strain of the yield platform was increased by 45.74%, which significantly reduced the height of the concrete compression zone.

(3) The yield platform length of HTRB630 steel bar was only 39.29% of that of HRB400 steel bars. The peak strain of HTRB630 steel bars was only 62.06% of that of HRB400 steel bars.

2.4 Test Setup and Instrumentation

The test used 1000kN-level MTS pseudo-static equipment to provide lateral load and a 1000kN jack to provide the axial pressure at the top of the column, as shown in Fig. 4. First, the specimen was hoisted near the MTS actuator and roughly adjusted the position of specimens according to the position of the vertical jack before starting the test. Second, the pressure beams on both sides were lowered and the compression beam was tightly pressed on the upper surface of the specimen base with special nuts. Third, the position of the MTS actuator was adjusted and the steel plate was fixed to the side of the column top with four screws. Finally, the position of the column top was adjusted sliding trolley to align with the center line of the column top, and the vertical jack height was slowly lower to prepare for the test. The column top lateral actuator and column top lateral force were automatically collected by the MTS device. The column top axial force was collected by a pressure sensor placed on the column top. A dial indicator was placed on the side of the specimen base to monitor the base displacement. By calibrating the specimen and MTS, the action surface of the lateral load coincided with the component plane, which controlled the out-of-plane deformation. During the test, the MTS actuator would have a slight angle change with the development of the plastic hinge at the

(a) Loading system and instrumentation

(b) The specimen under test

Fig. 4 Test setup.

Sun *et al. Int J Concr Struct Mater* (2022) 16:45

Page 7 of 28
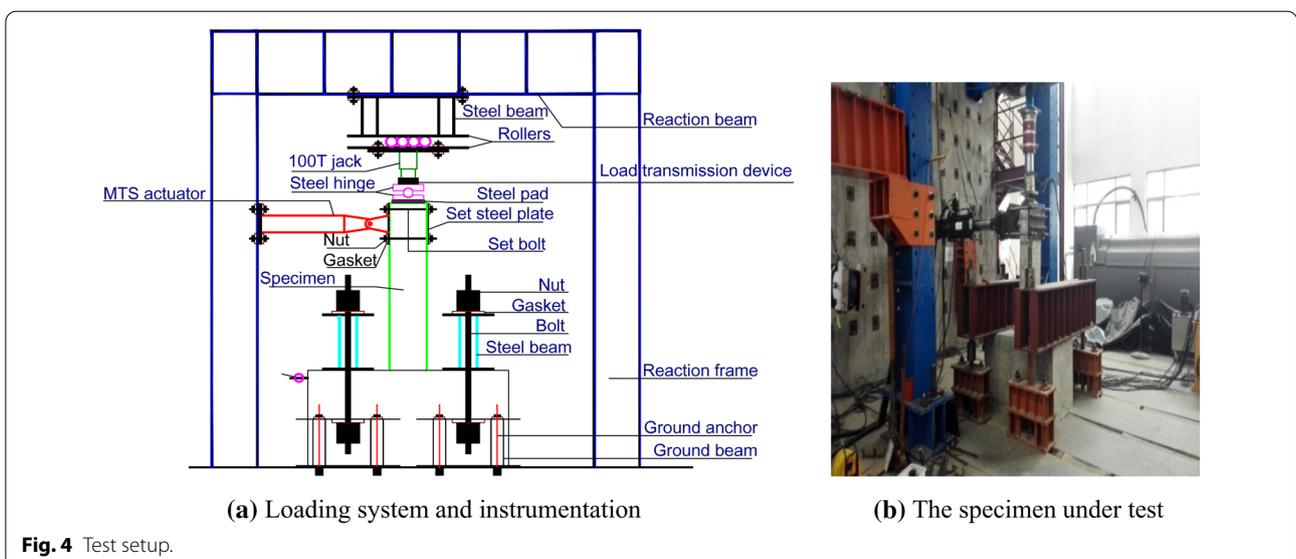
bottom of the column, but the angle was small, the measured force was not much different from its horizontal component. Fig. 5 gives the schematic diagram of the loading position. Rebar strain gauges were also arranged in the specimens to collect the reinforcement strains. The arrangement of strain gauges of specimens T60-1 ~ T60-5, T45-2, H45-2, H60-1, T45-3 and T45-4 are shown in Fig. 6. The other specimens were not arranged stain gauges. The DH3816 static strain test system was used to collect the strains.

2.5 Loading Protocol

The monotonically loaded skeleton curve of each specimen was simulated using the OpenSees software according to the mechanical properties of the material measured in the experiment, and then the yield load $P_{y,c}$ and yield displacement $\Delta_{y,c}$ were calculated. The calculation of yield load and ultimate load is shown in Fig. 7. The yield point Y was determined by the equivalent elasto-plastic energy method (Park, 1989), where the area of BYC was equal with that of OAB. The ultimate load was simply defined as 85% of maximum load, that was $P_u = 0.85P_{max}$ (Park, 1989). The variables P_y, P_{max}, and P_u indicated the yield load, maximum load, and ultimate load, respectively, while Δ_y, Δ_{max}, and Δ_u indicate the displacements at the yield, maximum, and ultimate loads, respectively. Characteristic points of the skeleton curve are shown in Fig. 7.

Table 5 shows numerical simulation and experimental results of yield loads and displacements. The simulated yield load was close to the measured yield load. There was a certain deviation between the simulated yield displacement and the measured yield displacement. Except specimen T45-1, the measured yield displacement of other specimens was basically within 80% of the corresponding simulated yield displacement. For most specimens, the influence of the deviation of loading displacement on the seismic performance of specimens was similar, and would not have a fundamental impact on the comparison conclusions. Therefore, the loading protocol in this article was appropriate and accurate.

(a) Longitudinal steel bars

(b) Stirrups

(c) Photograph

Fig. 6 Strain gauge arrangement.

Before the official loading, the axial and lateral forces were preloaded on the specimen. First, 20 kN axial force was applied through the vertical jack, and then 10 kN lateral force (P) with MTS actuator was applied for 10 min, then the nuts of the four screws with a wrench again was tightened to eliminate the gap between the fixed steel plate and the surface of the specimen. During pre-loading, the DH3816 system and the pressure sensor at the top of the column should be observed to ensure it could

Fig. 5 Top view of loading position.

Fig. 7 Characteristic points of the skeleton curve.

Sun *et al. Int J Concr Struct Mater*   (2022) 16:45

Page 8 of 28
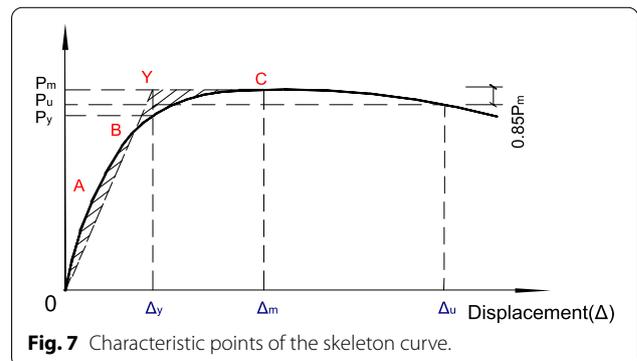
Table 5 Simulation and experimental results of specimens.

Specimen		Simulation results		Experimental results	
Number	Name	$P_{y,c}$ (kN)	$\Delta_{y,c}$ (mm)	P_y (kN)	Δ_y (mm)
1	T45-1	61.01	13.42	61.94	23.22
2	T60-1	73.42	6.71	85.10	5.86
3	T45-2	71.59	7.65	75.42	7.00
4	H45-1	57.06	8.06	56.10	7.42
5	H45-2	74.84	7.24	76.96	7.85
6	H60-1	85.03	6.61	92.60	6.29
7	T45-3	51.77	9.32	49.87	9.05
8	T45-4	73.17	8.45	75.06	8.24
9	T60-2	83.03	7.56	86.34	6.95
10	T45-5	65.80	9.98	67.19	8.39
11	T60-3	73.38	10.65	79.81	9.42
12	T60-4	80.87	6.99	78.40	6.22
13	T60-5	73.45	7.69	80.50	6.94

Fig. 8 Loading procedure.
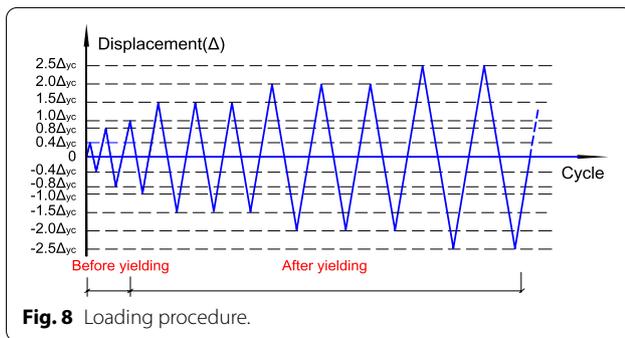
work normally. After the preloading was completed, the lateral force was removed and the axial force was increased to the design load. The magnitude of the axial force was monitored with a pressure sensor, and the formal loading of the lateral force was ready to begin.

The loading mode was displacement-controlled loading. The loading displacement amplitude at each load level was $0.4\Delta_{y,c} \cdot 0.8\Delta_{y,c} \cdot 1.0\Delta_{y,c} \cdot 1.5\Delta_{y,c} \cdot 2.0\Delta_{y,c} \cdot 2.5\Delta_{y,c} \cdot 3.0\Delta_{y,c}$... Each load level of the first three levels was cycled 1 time, and then each load level was cycled 3 times. The increment of displacement at each load level was $0.5\Delta_{y,c}$. The test was stopped when the ultimate load was less than 85% of the peak load of a cycle. The schematic diagram of the test loading path is shown in Fig. 8. Referring to the previous experience of using this loading device, the load control before yielding, the displacement control after yielding, and the subdivision change when approaching the predetermined yield point, as recommended in "Building Seismic Test Regulations JGJ/T 101-2015" (MOHURD, 2015) were not used. The main reasons are: (1) the test equipment must set a fixed

loading path before the test starts, and cannot be temporarily changed according to the yield point; (2) the "Yield of longitudinal steel bar as the yield point of the specimen" stipulated in MOHURD (2015) was not easily realized, because the strain gauges of longitudinal bars at each position did not necessarily yield at the same time.

3 Experimental results
3.1 Failure mode in Test Observations
3.1.1 CCC-CRs
CCC-CRs first appeared horizontal cracks at the bottom part of columns. With the increase of the loading displacement amplitude, horizontal through cracks appeared on the left and right sides, and multiple horizontal cracks on the front and back sides gradually developed, extended, developed diagonally, and intersected. After reaching the maximum lateral load, a small number of vertical cracks appeared near the corners of the rectangular column, the cover concrete on the left and right sides was spalled under 10 cm, and the cracks were basically uniform. The width of the main cracks on the left and right sides increased significantly, and the plastic hinge zone rotated significantly. The displacement amplitude continued to increase, the left and right sides increased, the spalling area of the cover concrete increased, the vertical cracks of the column bottom extended upwards, some edges and corners were crushed, the lateral load dropped gently to less than 85% of the maximum value, and the specimen was damaged.

The test phenomena of specimen H45-1 were recorded as follows. After the first cycle was loaded at $1.5\Delta_{y,c}$, the cracks were almost uniform, and the horizontal load began to drop; a vertical crack appeared on both sides of the back side, one extending 7 cm upwards, and the other extending about 10 cm obliquely upwards at 45 degrees (Fig. 9a). The width of the cracks on the back side of the column bottom was 2~3 mm. After the first cycle at $2.0\Delta_{y,c}$, the cover concrete of 25 cm^2 area on the left and right sides was spalled, and the back pedestal was crushed and spalled within 5 cm of the height (Fig. 9b). After the second cycle at $3.0\Delta_{y,c}$, the width of the main crack on the left reached 6 mm (Fig. 9c). The damage on the left side of the specimen after the test is shown in Fig. 9d. The concrete of the cover concrete below 10 cm was broken, and the stirrups and longitudinal bars were not completely exposed.

3.1.2 CCC-HRs
CCC-HRs first showed multiple horizontal cracks at bottom part of columns, and the crack spacing was slightly larger than that of CCC-CRs. As the amplitude of the loading displacement increases, horizontal penetration cracks appear on the left and right sides, and multiple

Sun *et al. Int J Concr Struct Mater*   (2022) 16:45

Page 9 of 28

(a) Cracks on the back side

(b) The cover concrete of the column bottom spalled

(c) Cracks on the left side

(d) Damage on the left side

Fig. 9 Test phenomenon photos of specimen H45-1.

horizontal cracks on the front and back sides gradually develop, extend, develop diagonally, and intersect. After reaching the maximum horizontal load, a few vertical cracks appeared near the corners of the rectangular column. The concrete near the main cracks began to peel and peel. The displacement amplitude continues to increase, the lateral load decreased step by step, the left and right sides become heavier, the spalling area of the cover concrete in the plastic hinge zone increased, and the main crack fully extended to the center. There were vertical splitting cracks with 40 cm high and developed diagonally upward on the edges and corners. Approaching the failure stage, the splitting cracks on the edges were crushed and spalled, and the exposed height of the column angle longitudinal bars reached about 35 cm. The longitudinal bars in the plastic hinge zone were buckled, the stirrups were exposed, and the concrete was completely crushed. The height could reach about 20 cm. The main crack extended inward about 10 cm, the lateral load dropped below 85% of the maximum value, and the specimen was broken.

The test phenomena of specimen T45-2 were recorded as follows. When the first cycle at $1.5\Delta_{y,c}$ was positively loaded, the lateral load reached the maximum value in the positive direction (about 71 kN), it began to drop slightly; the 75 cm^2 cover concrete on the left was slightly peeled (Fig. 10a); the width of the main crack at the height of 7 cm was 1.0 mm. After the third cycle at $2.5\Delta_{y,c}$, the

width of the main crack (4.8 mm) on the left continued to increase, the concrete cover concrete near the main crack was obviously spalled and uplifted, and the plastic hinge zone rotated obviously (Fig. 10b). After the first cycle at $3.5\Delta_{y,c}$, a vertical split with a height of 40 cm and a width of 6 mm appeared on the boundary edge of the front and left, and a vertical split with a height of 35 cm and a width of 5 mm also appeared at the boundary of the back and left. The bottom of the split extended 5 cm to the center, and a small piece of concrete was split quickly fragmentation, exposed and buckled corner longitudinal tendons (Fig. 10c). After the third cycle at $3.5\Delta_{y,c}$, the longitudinal bars below 30 cm in height on both sides of the left side were completely exposed, and the longitudinal bars at the bottom of the column were obviously buckled, the stirrups were exposed (Fig. 10d), and the cover concrete wad severely fragmented. The forward and reverse horizontal loads were reduced to 86% and 90% of the maximum value, considering that the longitudinal bars had been buckled, the test ended for safety reasons.

3.1.3 HCC-CRs
HCC-CRs first appeared horizontal cracks at the bottom part of columns. The average distance between the cracks was about 10 cm, which was less than that of common concrete columns. With the increase of the loading displacement amplitude, a number of horizontal cracks near the legs of the front and back
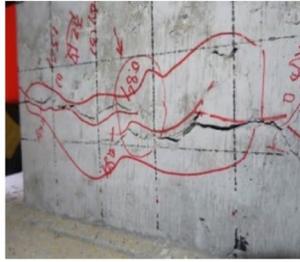
(a) The main crack on the left and the cover concrete spalled

(b) The main crack on the left and the uplift of the cover concrete

(c) Exposed longitudinal ribs at the junction of the front and left

(d) The longitudinal bars on both sides of the left side were exposed and buckled

Fig. 10 Test phenomenon photos of specimen T45-2.

sides gradually extended and intersected. The horizontal cracks developed obliquely but never formed oblique penetration cracks, and a few vertical cracks appeared near the leg legs. At this time, the longitudinal bars basically reach yield, and the lateral load was still increasing. After reaching the maximum lateral load, the longitudinal reinforcement was still in the yield stage, and the stirrup stress reached 35% of the yield stress. At this time, the number of vertical cracks near the corners of the column increased significantly, and the height increased significantly. The width of the main cracks near the height of 10 cm on the left and right sides continued to increase, and the concrete near the main cracks began to spall. The displacement amplitude continued to increase, the lateral load dropped rapidly, and the main cracks on the left and right sides were severely peeled. The edges and corners suddenly appeared about 60 cm vertical splitting cracks from the bottom of the column. Approaching the failure stage, the cleavage continues to bulge and crush. The bottom of the split crack gradually developed toward the center until it penetrated the spalling part, and the main crack extended to about 10 cm toward the center. The cover concrete below 30 cm on both sides was crushed and spalled, and the stirrups were exposed. At this time, the

stirrups were close to yielding, the lateral load drops below 85% of the maximum value, and the specimen was destroyed.

The test phenomena of specimen H60-1 were recorded as follows. When the first cycle at $2.0\Delta_{y,c}$ was reversely loaded, the concrete suddenly split vertically in the $15 \sim 60$ cm height range at the edge of the boundary between the back and the left (Fig. 11a), and the split width was about 3 mm. After the concrete crushed and fell off within the height of $12 \sim 30$ cm on the edge of the left junction, the splitting cracks at the junction between the back and the left increased and the outer bulge, and the bottom extended to about 10 cm to the center (Fig. 11b). The back side of the specimen after failure is shown in Fig. 11c. The main cracks on both sides at a height of 12 cm each extend 10 cm inward, the cross-section of the column was seriously weakened, and the height of the plastic hinge was about 15 cm. The crack width was about 3 mm. The damage to the right side of column bottom is shown in Fig. 11d. The damage height was higher than that of common concrete columns (about 20 cm), and the stirrups and longitudinal bars were exposed, and the damage was more serious than that of common concrete columns.

Sun *et al. Int J Concr Struct Mater* (2022) 16:45

Page 11 of 28
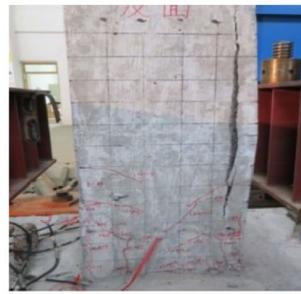
(a) Split at the junction between the back and the left

(b) Edge split at the junction between the back and the left

(c) The back side after failure

(d) Severely crushed in the plastic hinge zone of conrete on the right after failure

Fig.11 Test phenomenon photos of specimen H60-1.

3.1.4 HCC-HRs

HCC-HRs first appeared horizontal cracks at the bottom part of columns. As the loading displacement increased, horizontal through cracks appear on the left and right sides, and horizontal cracks on the front and back sides of the column bottom increase, extend, and pass through. A few vertical cracks appeared near the individual edge feet. At this time, the longitudinal reinforcement stress was about 30% of the yield stress. After the lateral load reached the maximum value, the horizontal cracks began to develop diagonally, and a number of cross diagonal cracks were formed on both sides. New horizontal through cracks continued to appear on the left and right sides, and large pieces spalled near the horizontal cracks at the column bottom. The vertical cracks on the edges of the column feet increased and developed upward, and some of the edge feet were crushed. At this time, the stress of the longitudinal reinforcement did not increase significantly. The displacement amplitude continued to increase, and vertical splitting cracks suddenly appeared about 70 cm upward from the bottom of the column near the corners, and the splitting cracks gradually developed to the center of the left and right sides, causing the

protection layers on the left and right sides to be large and uplifted. At this time, the stress of the longitudinal reinforcement increases rapidly to reach the yield stress, and the lateral load reached the maximum value and began to decrease. Close to the failure stage, the concrete blocks split by the split cracks were raised and crushed, and the cover concrete of large concrete below 50 cm was broken and peeled, and the stirrups and longitudinal bars were exposed. The hysteresis curve jittered and quickly dropped below 85% of the maximum value. At this time, the longitudinal bars were still in the yielding stage, and the test ended.

The test phenomena of specimen T60-3 were recorded as follows. After the first cycle was loaded at $2.0\Delta_{y,c}$, the cover concrete under the height of 10 cm on the left was spalled; vertical splitting crack with a width of 1 cm and a height of 70 cm appeared on the edges at the junction of the front and the right (Fig. 12a). A 25 cm high vertical splitting crack also appeared on the edge of the junction between the back and the right. Most of the cover concrete below the 45 cm height on the right was severely peeled and swelled. After the second cycle loaded, the concrete column split from the edge at the junction of

(a) Vertical crack at the edge of the border between the front and the right

(b) Split cracks and uplift of the cover concrete on the right

(c) The cover concrete below 70 cm on the left was crushed in one piece

(d) The cover concrete below 50 cm on the right was crushed in one piece

Fig. 12 Test phenomenon photos of specimen T60-3.

the front and the right and the uplifted concrete cover concrete on the right suddenly bulged and crushed, and the cover concrete below 50 cm on the right was all crushed and fallen off (Fig. 12b), stirrups and longitudinal bars were exposed. The damage on the left of the specimen after failure is shown in Fig. 12c. The damage on the right side of the specimen is shown in Fig. 12d. The main cracks near the height of 15 cm extended about 5 cm from both sides to the center of the column. The left and right sides of the concrete were below 50 cm in height. The cover concrete was peeled off and crushed in pieces, and the damage height was more serious than that of HCC-CRs.

3.1.5 CHCCs
CHCCs first appeared horizontal cracks at the bottom part of columns. With the increase of the loading displacement, horizontal through cracks appeared on the left and right sides, and the horizontal cracks at the bottom of the front and back sides increased, extended, and passed through, and a few vertical cracks appeared near the individual edge feet. The displacement amplitude continued to increase, the horizontal cracks began to develop diagonally, and the vertical cracks near the

corners of the column obviously increased and developed upward. There were multiple horizontal through cracks on the left and right sides, the main crack was formed at the height of about 10 cm at the bottom of the column, and the cover concrete near the main crack was peeled. At this time, the high-strength longitudinal reinforcement was close to yielding, and the stirrup stress reached 30% of the yield stress, and the horizontal bearing capacity of the specimen could continue to increase. The horizontal displacement continued to increase, and vertical splitting cracks suddenly appeared on multiple edges of the specimen. The cracks extended from the bottom of the column to a height of about 60 cm. The horizontal bearing capacity reached the maximum. At this time, the high-strength longitudinal reinforcement was in the yield stage, and the strain of the high-strength stirrups increased to about 35% of the yield stress. The loading amplitude continued to increase, and the small prisms formed by the splitting cracks near the edges and corners gradually bulged, crushed, and peeled off, and the hysteresis curve slightly jitters and drops significantly. Near the failure stage, the splitting cracks significantly reduced the column section, the main cracks obviously

extended to the center of the column, and the concrete crushing area expanded from the area above the main crack to the area between the main crack and the base. The horizontal bearing capacity further decreased, and the test ended. At this time, the longitudinal reinforcement was still in the yield stage, and the stress of the high-strength stirrup was about 65% of the yield stress.

The test phenomena of specimen T60-5 were recorded as follows. When the first cycle at $2.0\Delta_{y,c}$ was loaded, the edges on both sides of the back suddenly appeared 65 cm and 50 cm high vertical splitting cracks, the width of the cracks was about 1 mm (Fig. 13a). After the end of the second cycle at $2.5\Delta_{y,c}$, the edge between the back and the right side was crushed and fell off within $10 \sim 60$ cm, and the bottom of the falling body extended 5 cm to the center of the column (Fig. 13b), the width of the crack was about 1 mm. After the first cycle at $3.5\Delta_{y,c}$, the crushed area of the cover concrete expanded from the main crack with a height of 10 cm to the column bottom (Fig. 13c), the main crack extended to the center of the column, and the plastic hinge zone rotated significantly. Fig. 13d shows the damage of the column bottom. The main crack near the height of 10 cm extended to the center of the column. The cover concrete of concrete below 30 cm on the left and right sides was broken, and the damage height was smaller.

Based on the above analysis, it could be seen that the failure modes of specimens were all bending failures. The columns had roughly gone through the following stages: horizontal cracks at the bottom of the tensioned side column developed, extended obliquely, and cross through. The cover concrete near the main crack at the bottom of the left and right columns peeled and peeled off. Vertical cracks at the bottom of the column occurred and developed. The plastic hinge zone was severely crushed, and the lateral load dropped to 85% of the maximum load. Compared with common concrete columns, high-strength concrete columns had the characteristics of large penetration depth of main cracks, severe plastic damage in the plastic hinge zone, and high concrete damage in the cover concrete. They also had higher vertical split cracks before failure. As a result, the concrete cover concrete bulges and crushes, and the longitudinal reinforcements at the bottom of the column were obviously buckled, which indicated the brittleness of high-strength concrete. High-strength confined stirrups effectively could reduce the massive uplift of the concrete cover concrete caused by vertical splitting of edges, restrict the diagonal development of splitting cracks in the column bottom area to the column center, and effectively delay the compression buckling after the longitudinal bars were exposed.

(a) Vertical splitting cracks on both sides of the back

(b) Crushed edges at the junction between the back and the right

(c) The crushing area expanded to the column bottom

(d) The bottom of the column after faliure

Fig. 13 Test phenomenon photos of specimen T60-5.

Sun *et al. Int J Concr Struct Mater* (2022) 16:45

Page 14 of 28

3.2 Hysteresis Curves of Load Displacement

Hysteresis loops of lateral load–displacement relationship are shown in Fig. 14. The loading was ended when the later load in any direction was lower than 85% of the peak strength during the test. There was a case, where the lateral strength in the other direction did not drop to 85% of the maximum load, which may be induced asymmetric behavior of hysteresis curves between the positive and negative loading direction occurred in Fig. 14. In addition, the measured hysteresis curve was affected by various factors, and there were certain differences in the seismic performance of the forward and reverse directions. The other two reasons for it were as follows. (1) The specimen was subjected to continuous eccentric compressive load for 100 days from the age of 28 days. The concrete in the compression zone would creep, and the compressed steel bar would generate pre-compression stress. Thus, the reverse loading stiffness and peak load were improved. (2) The accumulation of damage was also related to the loading path.
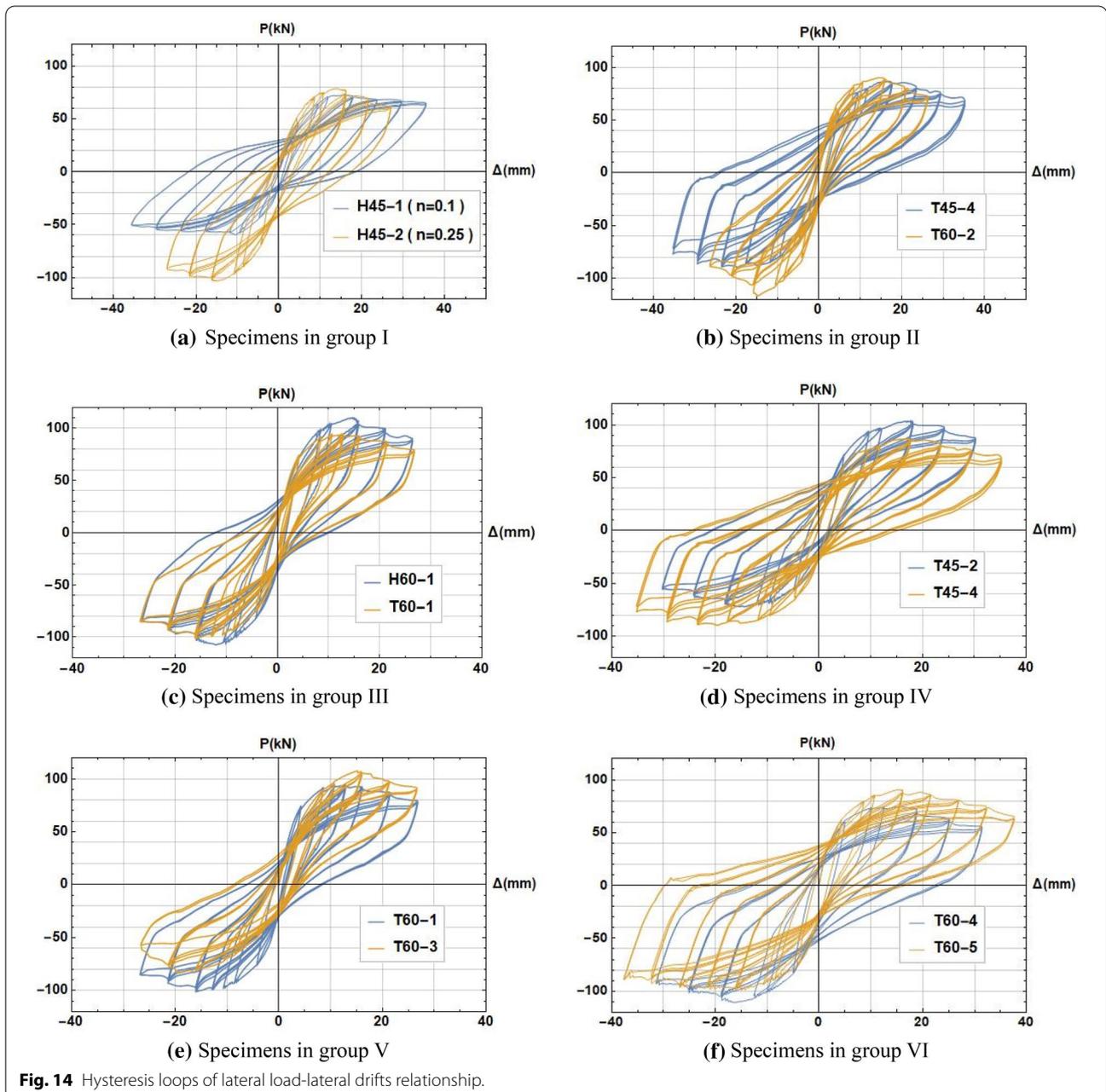
Fig. 14 Hysteresis loops of lateral load-lateral drifts relationship.

Sun *et al. Int J Concr Struct Mater* (2022) 16:45

Page 15 of 28

After the crack developed, the two directions would not be exactly the same.

Hysteresis loops were all bow-shaped, and the specimens had good ductility and energy dissipation capacity. The lateral load drop section of C45 concrete columns was gentler, the pinch phenomenon was slight, and the area surrounded by the hysteresis loop was large. C60 concrete columns had a large lateral strength, but the lateral load decreased rapidly, the pinch phenomenon was obvious, and the area surrounded by the hysteresis loop was small. The ductility and energy dissipation capacity of C60 concrete columns were not as good as C45 concrete columns. No matter whether it was a common or high-strength concrete column, after the equal strength of longitudinal high-strength reinforcements, the strength of specimens was similar, and the shape of the hysteresis curve was not changed significantly. Using high-strength stirrups to confine high-strength concrete, although it could not significantly improve the lateral strength of columns, it could significantly reduce the descent speed of the strength degradation, expand the area surrounded by the hysteresis loop, and effectively improve the ductility and energy dissipation capacity of high-strength concrete columns.

4 Analysis and Discussion of Effect on the Seismic Performance of Specimens

4.1 Seismic Performance Indicators

4.1.1 Lateral Strength

The skeleton curve is an important basis for determining the characteristic points of the restoring force model of the component. The skeleton curve and three characteristic points of Specimen H45-1 are shown in Fig. 11. Divide the load and lateral displacement of each point on the skeleton curve by the yield load and yield displacement of the specimen, respectively, to obtain a dimensionless normalized skeleton curve, that is, the P/P_y-Δ/Δ_y curve. Lateral strength is an important indicator of reinforced concrete members and an important characteristic point on the skeleton curve, including the yield load, maximum load, and ultimate load, as shown in Fig. 15.

4.1.2 Displacement Ductility

Ductility is also an important index for reinforced concrete members, reflecting the ability of specimens to deform without a significant decrease in strength. The displacement ductility coefficient is

$$\mu = \Delta_u / \Delta_y \tag{1}$$

4.1.3 Energy Dissipation Capacity

The normalized cumulative hysteretic energy coefficient E_N was used in this study as the indexes to evaluate the energy

Fig. 15 Skeleton curve and characteristic points of specimen H45-1.
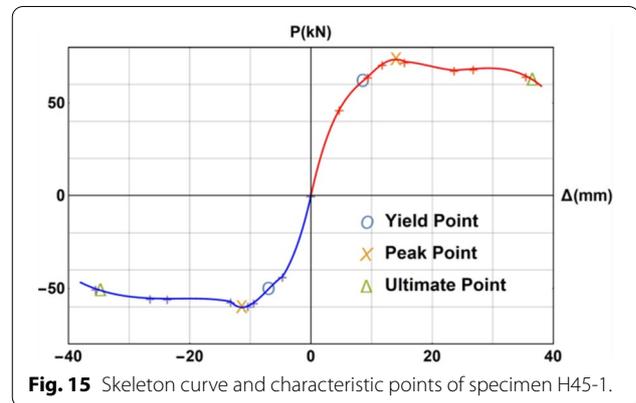
dissipated capacity of the specimens. E_N reflects the growth of the total energy absorbed by the component under the repeated action of the earthquake. $E_{N,m}$ is the cumulative hysteretic energy consumption coefficient of the component at the end of the *m*th loading cycle (Li et al., 2019), the formula of it was given as

$$E_{N,m} = \frac{1}{P_y \Delta_y} \sum_{i=1}^{m} S_i \tag{2}$$

where S_i is the area surrounded by the *i*th hysteresis loop (that is, the area of the shaded part in Fig. 16).

4.1.4 Stiffness Degradation

The stiffness degradation, which is caused by cracking, yielding of reinforcements, bond-slipping between steel and concrete, is an important index to reflect the level of damage of the columns. In low-cycle repeated tests, the loop stiffness K can be used to measure the overall stiffness of all cycles under the same amplitude. To facilitate comparison, the loop stiffness of the forward and reverse loops at the same displacement was averaged. K_j is the stiffness of the loop under the *j*th displacement amplitude (Li et al., 2019) and its formula is

$$K_j = \frac{\sum_{i=1}^{n} P_j^i}{\sum_{i=1}^{n} \Delta_j^i} \tag{3}$$

where P_j^i and Δ_j^i are the maximum horizontal load and displacement amplitude of the *i*th cycle under the *j*th displacement amplitude; *n* is the total number of loading cycles of the *j*th displacement amplitude.

4.1.5 Strength Degradation

In the quasi-static test, with the increase of the loading displacement amplitude increased, the column gradually entered the elasto-plastic phase from the elastic phase,

Fig. 16 Schematic of the area enclosed by the *i*th hysteresis loop.
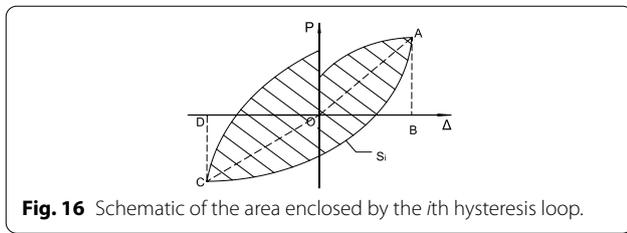
and its stiffness and strength also deteriorated. The strength degradation can be expressed by the strength degradation coefficient λ, as shown in Formula (4):

$$\lambda_i^j = \frac{P_j^i}{P_j^1} \qquad (4)$$

where λ_i^j is the strength degradation coefficient of the *i*th cycle under the *j*th displacement amplitude.

4.2 Effect of Axial Load Ratio

Fig. 17 gives the normalized skeleton curves of specimens in group I. It could be seen from that the influence of the axial load ratio was mainly reflected in the descending section of the curve. Before the yield displacement, the P/P_y-Δ/Δ_y curves of each specimen almost overlapped. After reaching the maximum load, the P/P_y-Δ/Δ_y curve of

Fig. 17 Normalized skeleton curves of specimens in group I.
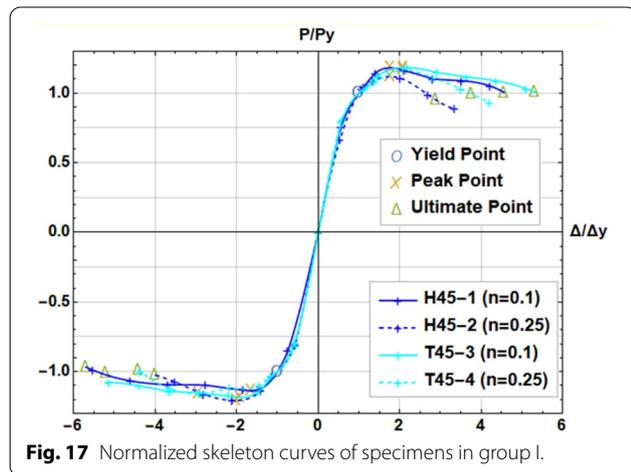
the specimen with the axial load ratio of 0.25 decreased faster and reached the ultimate load quickly.

The lateral strength and displacement ductility coefficient for specimens with different axial load ratio are shown in Table 6. After the axial load ratio was increased from 0.1 to 0.25, the yield load, maximum load, and failure load were increased by about 37% of specimens (H45-1 and H45-2) with HRB400 reinforcements. For specimens (H45-3 and H45-4) with HTRB630 reinforcements, the lateral strength were increased more greatly, reaching about 48%, indicating that increasing the axial load ratio in a certain range was beneficial to the lateral strength of concrete columns. Compared with specimens H45-1 and H45-2, the diameter of longitudinal reinforcements of specimen T45-3 was smaller and the spacing of stirrups was larger; compared with specimens T45-3, the axial load of specimen T45-3 was smaller, so the strength of specimen T45-3 was lower. The yield displacement did not change much, the maximum displacement was increased by about 15%, and the failure displacement was decreased by about 28%. The displacement ductility coefficient μ of the four specimens were all above 3. The displacement ductility coefficient μ of the specimens with HRB400 reinforcements and the specimens with HTRB630 reinforcements were decreased by 22.2% and 32.9%, respectively, indicating that the increase of the axial load ratio significantly reduced the ductility of specimens.

Fig. 18a gives the cumulative hysteretic energy coefficient E_N curves of specimens in group I. Before approaching the limit displacement, the cumulative energy dissipation of the specimen with high axial load ratio was larger than that of the specimen with lower axial load ratio at the same displacement ductility. However, the difference between the two kinds of specimens gradually decreased with the increase of the displacement ductility.

Fig. 18b gives the average loop stiffness K curves of specimens in group I. The energy dissipation capacity and stiffness of specimens with high axial load ratio at the same displacement ductility were obviously improved, but after the maximum load, the stiffness decreases rapidly.

Table 7 shows the strength degradation coefficients of the four specimens in control group I. The strength

Table 6 Lateral strength and displacement ductility coefficient of specimens in group I.

Specimen	n	A_s	A_{sv}	P_y (kN)	Δ_y (mm)	P_{max} (kN)	Δ_{max} (mm)	P_u (kN)	Δ_u (mm)	μ
H45-1	0.10	4C18	C8@100(2)	56.10	7.42	65.14	12.69	55.37	37.48	5.13
H45-2	0.25	4C18	C8@100(2)	76.96	7.85	89.75	14.77	76.29	26.92	3.44
T45-3	0.10	4D14	D8@150(2)	49.87	9.05	59.00	18.10	50.15	47.57	5.26
T45-4	0.25	4D14	D8@150(2)	75.06	8.24	87.36	20.68	74.26	33.68	4.09

Fig. 18 Seismic performance of specimens in group I.
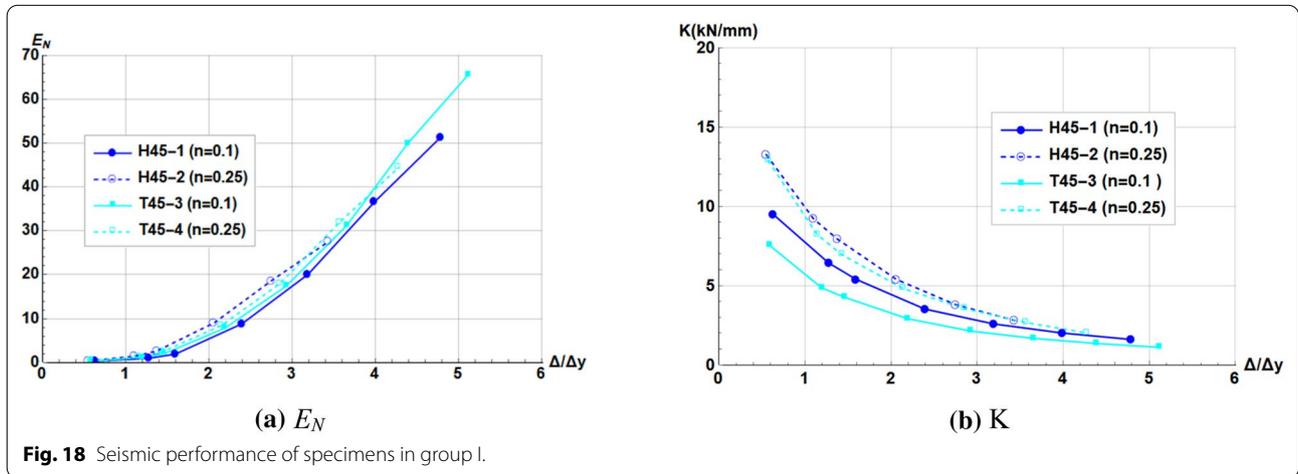
Table 7 Strength degradation coefficient of specimens in control group I

Specimen	Δ/Δ_y	λ			Specimen	Δ/Δ_y	λ		
		Cycle 1	Cycle 2	Cycle 3			Cycle 1	Cycle 2	Cycle 3
H45-1 ($n=0.10$)	2.39	1.000	0.983	0.977	H45-2 ($n=0.25$)	2.06	1.000	0.970	0.957
	3.19	1.000	0.995	0.988		2.75	1.000	0.984	0.969
	3.99	1.000	0.984	0.972		3.44	1.000	0.989	–
	4.79	1.000	0.993	–					
T45-3 ($n=0.10$)	2.19	1.000	0.983	0.975	T45-4 ($n=0.25$)	2.14	1.000	0.990	0.985
	2.92	1.000	0.985	0.979		2.85	1.000	0.982	0.966
	3.65	1.000	0.985	0.980		3.56	1.000	0.973	0.951
	4.38	1.000	0.984	0.971		4.27	1.000	0.953	–
	5.12	1.000	0.972	–					

degradation coefficient of each specimen was greater than 0.95. The strength of the specimen degraded slightly (< 5%) with the increase of the number of cycles at the same displacement amplitude. Therefore, the effect of the axial load ratio on the strength degradation coefficient was not obvious.

4.3 Effect of Concrete Grade
Fig. 19 gives the normalized skeleton curves of specimens in group II. The influence of concrete grade was mainly reflected in the descending section after reaching the maximum point. Before the yield displacement, the P/P_y-Δ/Δ_y curves of each specimen were similar. In the descending section after the maximum load, the P/P_y-Δ/Δ_y curve of the high-strength concrete column decreased faster and reached the ultimate load quickly, which reflected the brittleness of the high-strength concrete material.

The lateral strength and displacement ductility coefficient of specimens in group II are shown in Table 8. Increasing the concrete grade from C45 to C60, the yield

load, maximum load and ultimate load of specimens H45-2 and H60-1 were increased by about 13% ~ 19%; the yield displacement was reduced by about 16–19% except for specimen T60-3, the maximum displacement was

Fig. 19 Normalized skeleton curves of specimens in group II.

Sun *et al. Int J Concr Struct Mater*   (2022) 16:45

Page 18 of 28
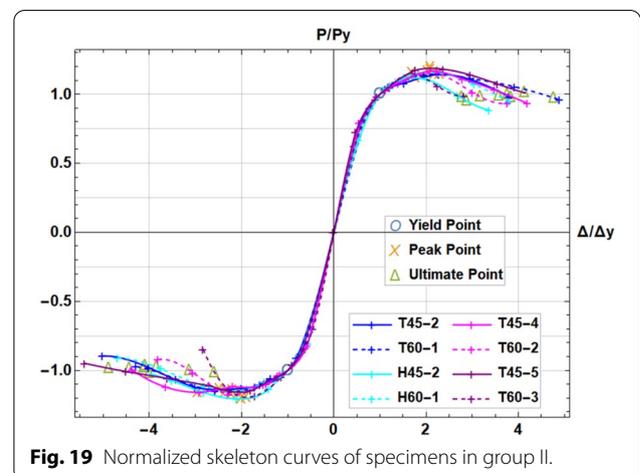
Table 8 Lateral strength and displacement ductility of specimens in group II.

Specimen	Concrete	n	A_s	A_{sv}	P_y (kN)	Δ_y (mm)	P_{max} (kN)	Δ_{max} (mm)	P_u (kN)	Δ_u (mm)	μ
T45-2	C45	0.25	4D14	C8@100(2)	75.42	7.00	86.16	16.58	73.23	27.66	3.97
T60-1	C60	0.25	4D14	C8@100(2)	85.10	5.86	97.94	13.30	83.25	25.92	4.44
H45-2	C45	0.25	4C18	C8@100(2)	76.96	7.85	89.75	14.77	76.29	26.92	3.44
H60-1	C60	0.25	4C18	C8@100(2)	92.60	6.29	106.84	13.26	90.81	23.26	3.71
T45-4	C45	0.25	4D 14	D8@150(2)	75.06	8.24	87.36	20.68	74.26	33.68	4.09
T60-2	C60	0.25	4D14	D8@150(2)	86.34	6.95	100.70	15.25	85.60	21.92	3.15
T45-5	C45	0.25	4D14	D8@100(2)	67.19	8.39	78.87	17.44	67.04	37.19	4.51
T60-3	C60	0.25	4D14	D8@100(2)	79.81	9.42	93.25	16.88	79.26	25.27	2.68

reduced by about 10–26%, and the ultimate displacement was reduced by about 6–34%. Except specimen T60-3, the displacement ductility coefficients μ of the other three specimens with C60 concrete were all above 3.

Fig. 20a gives the cumulative hysteretic energy coefficient E_N curves of specimens in group II. Except for specimens T45-5 and T60-3, the cumulative hysteresis energy dissipation of high-strength concrete specimens was much lower than that of common concrete specimens with the same displacement ductility.

Fig. 20b gives the average loop stiffness K curves of specimens in group II. With the same displacement ductility, the loop stiffness of the C60 concrete specimens was greater than that of C45 concrete specimens. The stiffness degradation rate of C60 concrete columns was faster than that of C45 concrete columns.

Table 9 shows the strength degradation coefficients of specimens in control group II. The strength degradation coefficient of each specimen was greater than 0.95. The strength of the specimen degraded slightly (<5%) with the increase of the number of cycles at the same displacement amplitude. Therefore, the effect of the concrete

grade on the strength degradation coefficient was not obvious.

4.4 Effect of Equal Strength Substitution of Longitudinal Reinforcements

Fig. 21 gives the normalized skeleton curves of specimens in group III. The influence of equal strength substitution of longitudinal reinforcements was mainly reflected in the descending section. Before the yield displacement, the P/P_y-Δ/Δ_y curves of the specimens were similar. In the descending section after the maximum load, the specimens with HTRB630 longitudinal reinforcement descended slowly, which was more obvious in the positive direction of loading.

The lateral strength and displacement ductility coefficient of specimens in group III are shown in Table 10. The equal strength replacement of longitudinal reinforcements has little effect on the lateral strength of the specimens. The displacement ductility coefficients μ of the four specimens were all above 3, indicating that whether it was common concrete C45 or high-strength concrete C60, HTRB630 high-strength reinforcements could work

Fig. 20 Seismic performance of specimens in group II.

Sun *et al. Int J Concr Struct Mater* (2022) 16:45

Page 19 of 28
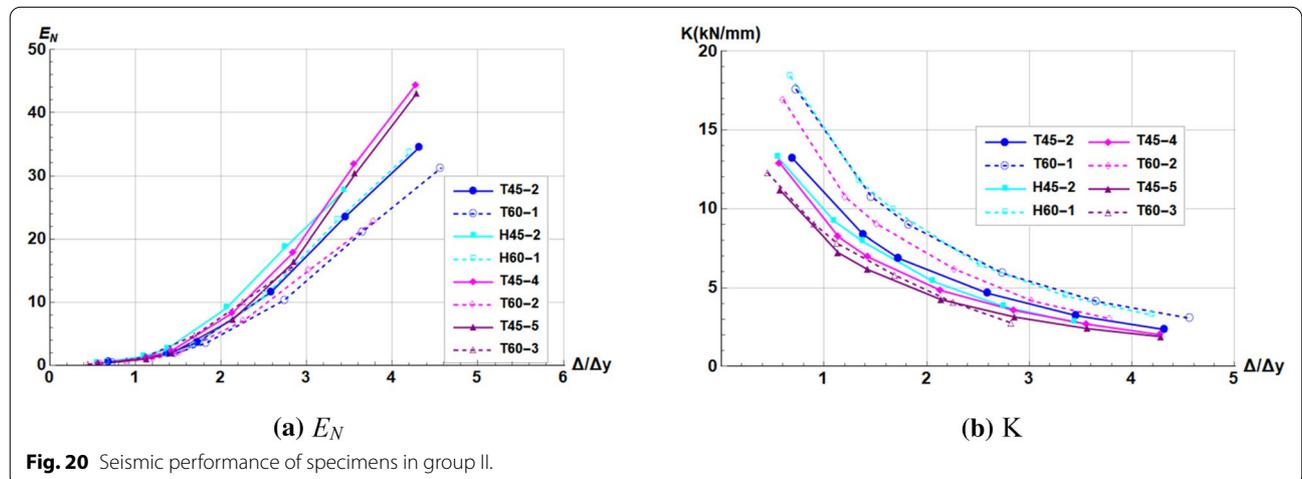
Table 9 Strength degradation coefficient of specimens in control group II.

Specimen	Δ/Δ_y	λ			Specimen	Δ/Δ_y	λ		
		Cycle 1	Cycle 2	Cycle 3			Cycle 1	Cycle 2	Cycle 3
T45-2 (C45)	2.59	1.000	0.984	0.968	T60-1 (C60)	2.74	1.000	0.983	0.977
	3.46	1.000	0.987	0.973		3.65	1.000	0.980	0.972
	4.32	1.000	0.979	-		4.57	1.000	0.989	-
H45-2 (C45)	2.06	1.000	0.970	0.957	H60-1 (C60)	2.52	1.000	0.973	0.949
	2.75	1.000	0.984	0.969		3.36	1.000	0.985	0.981
	3.44	1.000	0.989	-		4.20	1.000	1.001	-
T45-4 (C45)	2.14	1.000	0.990	0.985	T60-2 (C60)	2.27	1.000	0.962	0.956
	2.85	1.000	0.982	0.966		3.03	1.000	1.002	0.996
	3.56	1.000	0.974	0.951		3.79	1.000	0.987	-
	4.27	1.000	0.953	-					
T45-5 (C45)	2.14	1.000	0.987	0.985	T60-3 (C60)	1.70	1.000	0.992	0.991
	2.86	1.000	0.994	0.991		2.26	1.000	0.987	0.977
	3.57	1.000	0.991	0.982		2.83	1.000	0.988	-
	4.29	1.000	0.988	-					
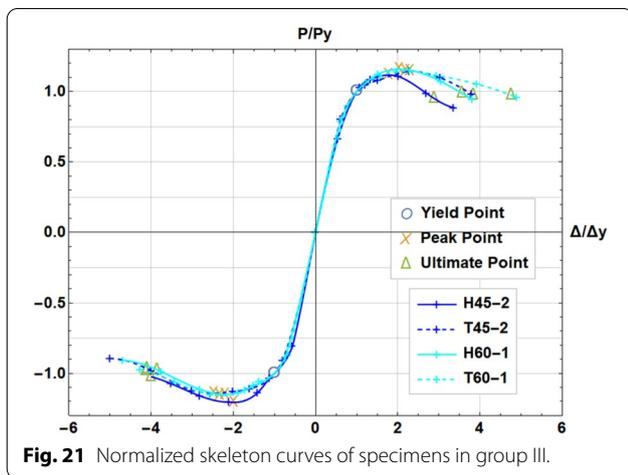
Fig. 21 Normalized skeleton curves of specimens in group III.

well. The displacement ductility coefficients of C45 concrete specimens and high-strength concrete C60 specimens were increased by 15.41% and 19.68%, respectively, indicating that the specimens with high-strength reinforcements had better displacement ductility when used in conjunction with C60 high-strength concrete.

Fig. 22a gives the cumulative hysteretic energy coefficient E_N curves of specimens in group III. In the initial stage of displacement loading, there was little difference in the cumulative energy dissipation of specimens before and after the equal strength substitution of longitudinal reinforcements. When the displacement increased to a certain degree, HRB400 steel bar gradually entered yield, and the energy dissipation capacity of the specimen was significantly enhanced. Replacing HRB400 reinforcements with HTRB630 reinforcements, the total accumulated energy dissipation of C45 concrete specimens was increased by 25.27%, and that of the C60 concrete specimens was decreased by 7.09%.

Fig. 22b gives the average loop stiffness K curves of specimens in group III. Equal strength substitution of longitudinal reinforcements had little effect on the stiffness of specimens. The degradation trends of the specimens were exactly the same, and the stiffness was similar. The errors of the average loop stiffness of those specimens were within 10%.

Fig. 22c shows the rebar strain envelop curves of specimens in group III. In Fig. 17c, yield strains of HRB400 and HTRB630 reinforcements were marked with

Table 10 Lateral strength and displacement ductility of specimens in group III.

Specimen	Concrete	n	A_s	A_{sv}	P_y (kN)	Δ_y (mm)	P_{max} (kN)	Δ_{max} (mm)	P_{ult} (kN)	Δ_{ult} (mm)	μ
H45-2	C45	0.25	4C18	C8@100(2)	76.96	7.85	89.75	14.77	76.29	26.92	3.44
T45-2	C45	0.25	4D14	C8@100(2)	75.42	7.00	86.16	16.58	73.23	27.66	3.97
H60-1	C60	0.25	4C18	C8@100(2)	92.60	6.29	106.84	13.26	90.81	23.26	3.71
T60-1	C60	0.25	4D14	C8@100(2)	85.10	5.86	97.94	13.30	83.25	25.92	4.44

(a) E_N

(b) K

(c) Rebar strain
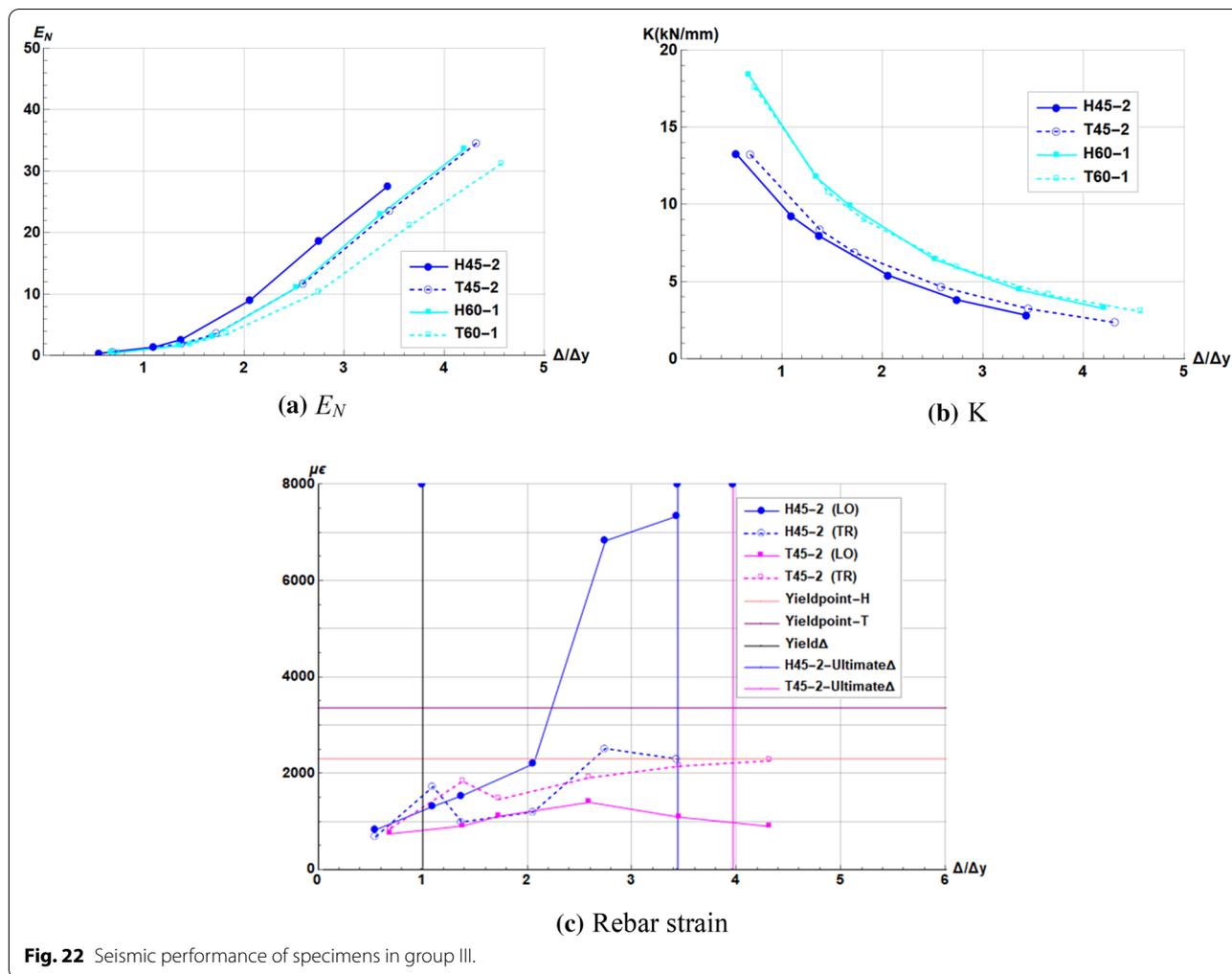
Fig. 22 Seismic performance of specimens in group III.

horizontal lines; the yield and ultimate displacements of specimens H45-2 and T45-2 were marked with a vertical line; "LO" represents longitudinal reinforcements; "TR" represents transverse reinforcements. The strain of HRB400 longitudinal reinforcements was increased with the increase of the loading displacement, and it entered yielding at about $2\Delta y$, and the strain reached about $7300\mu\varepsilon$ when the specimen failed. The strain of HTRB630 longitudinal reinforcements was below $1400\mu\varepsilon$, and the longitudinal reinforcements had not yet yielded at the time of failure. Under the condition of repeated loading, the HTRB630 longitudinal reinforcements could the yield point of steel bars, the concrete was crushed, and the HTRB630 longitudinal reinforcements and the concrete reached the failure state at the same time, giving full play to the seismic capacity of the reinforced concrete column.

Table 11 shows the strength degradation coefficients of specimens in control group III. The strength degradation coefficient of each specimen was greater than 0.94. The strength of the specimen degraded slightly (< 6%) with the increase of the number of cycles at the same displacement amplitude. Therefore, the effect of equal strength substitution of longitudinal reinforcements on the strength degradation coefficient was not obvious.。

4.5 Effect of Equal Strength Substitution of Stirrups

Fig. 23 gives the normalized skeleton curves of specimens in group IV. The effect of equal strength substitution of stirrups was different due to the different grades of concrete. For C45 concrete specimens, the normalized skeleton curves of the two specimens almost completely overlap. For C60 concrete specimens, the part of the normalized skeleton curve before the maximum point was almost the same, and the drop rate of the high-strength stirrup specimen after the maximum point was faster.

The lateral strength and displacement ductility coefficient of specimens in group IV are shown in Table 12.

Sun *et al. Int J Concr Struct Mater*   (2022) 16:45

Page 21 of 28

Table 11 Strength degradation coefficient of specimens in control group III.

Specimen	Δ/Δ_y	λ			Specimen	Δ/Δ_y	λ		
		Cycle 1	Cycle 2	Cycle 3			Cycle1	Cycle 2	Cycle 3
H45-2 (HRB400)	2.06	1.000	0.970	0.957	T45-2 (HTRB630)	2.59	1.000	0.984	0.968
	2.75	1.000	0.984	0.969		3.46	1.000	0.987	0.973
	3.44	1.000	0.989	–		4.32	1.000	0.979	–
H60-1 (HRB400)	2.52	1.000	0.973	0.949	T60-1 (HTRB630)	2.74	1.000	0.983	0.977
	3.36	1.000	0.985	0.981		3.65	1.000	0.980	0.972
	4.20	1.000	1.001	–		4.57	1.000	0.989	–
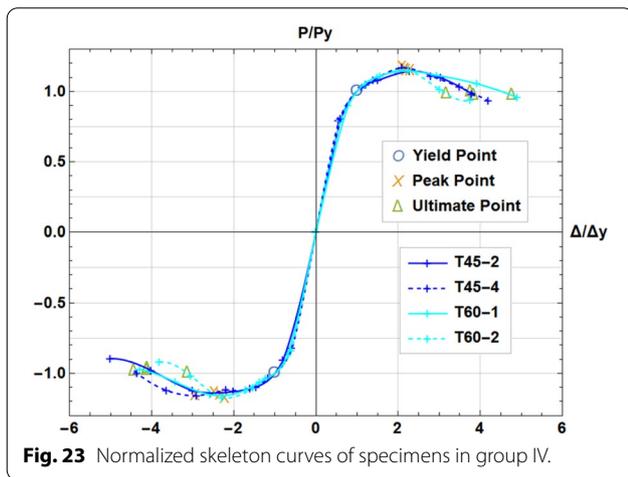
Fig. 23 Normalized skeleton curves of specimens in group IV.

Equal strength substitution of stirrups had little effect on the lateral strength of specimens. The displacement ductility coefficient μ of the four specimens were all above 3, indicating that whether it was C45 concrete or C60 concrete, HTRB630 high-strength stirrups could play an effective confinement role. The effect of equal-strength substitution of stirrups on the ductility of the specimen was related to the "efficiency" of the confinement of the stirrups. The practice of equal strength substitution of the stirrups by increasing the spacing of the stirrups reduces the confining effect of the stirrups to a certain extent.

Fig. 24a gives the cumulative hysteretic energy coefficient E_N curves of specimens in group IV. In the initial stage of displacement loading, the equal strength substitution of stirrups had little effect on the cumulative energy dissipation of specimens. In the middle and late stage of displacement loading, the cumulative energy dissipation capacity of the specimens at the same displacement ductility was improved, but the increase was related to the concrete grades. After the common stirrups were replaced with high-strength stirrups, the total energy dissipation of high-strength concrete specimens was decreased by 26.79%.

Fig. 24b gives the average loop stiffness K curves of specimens in group IV. The stiffness of the specimen decreased after equal strong substitution of stirrups. The degradation trend of the curves of the two specimens in the two groups was exactly the same. The spacing of stirrups of specimen T45-2 was larger than that of specimen T45-1, and the spacing of stirrups of specimen T60-2 was larger than that of specimen T60-1, so the average loop stiffness of the specimens with high-strength stirrups was slightly lower than that of the specimens with common stirrups at the same displacement ductility.

Fig. 24c shows the rebar strain envelop curves of specimens in group IV. The strain gauges of longitudinal reinforcements of specimen T45-4 were damaged when they were close to failure, and the strain of the last level in the figure was recorded as 0. In the early stage of displacement loading, the longitudinal reinforcements and stirrup strains of the specimens with high-strength stirrups were smaller than those of the specimens with common stirrups, which could explain ξ_{eq} of specimens with HTRB630 stirrups were lower when the displacement was small. When the specimens were damaged, the

Table 12 Lateral strength and displacement ductility of specimens in group IV.

Specimen	Concrete	n	A_s	A_{sv}	P_y (kN)	Δ_y (mm)	P_{max} (kN)	Δ_{max} (mm)	P_u (kN)	Δ_u (mm)	μ
T45-2	C45	0.25	4D14	C8@100(2)	75.42	7.00	86.16	16.58	73.23	27.66	3.97
T45-4	C45	0.25	4D14	D8@150(2)	75.06	8.24	87.36	20.68	74.26	33.68	4.09
T60-1	C60	0.25	4D14	C8@100(2)	85.10	5.86	97.94	13.30	83.25	25.92	4.44
T60-2	C60	0.25	4D14	D8@150(2)	86.34	6.95	100.70	15.25	85.60	21.92	3.15

Sun *et al. Int J Concr Struct Mater*   (2022) 16:45

Page 22 of 28

(a) E_N

(b) K

(c) Rebar strain
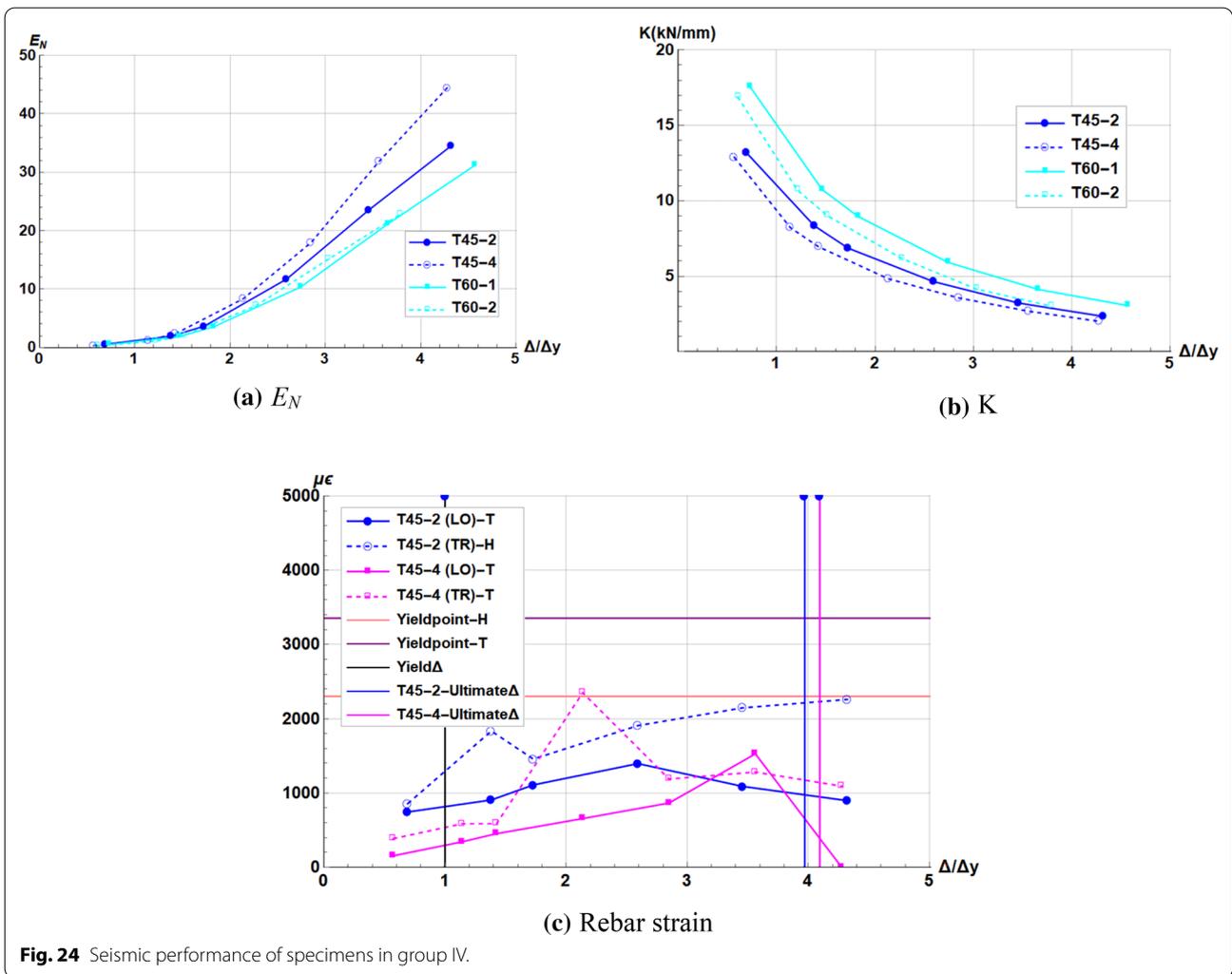
Fig. 24 Seismic performance of specimens in group IV.

stirrup of the specimen T45-2 was close to yield, and the stirrup strain of the specimen T45-4 was less than half of the yield strain, indicating that the high-strength stirrup still had a large strength reserve and safety degree when the specimen was damaged.

Table 13 shows the strength degradation coefficients of specimens in control group IV. The strength degradation coefficient of each specimen was greater than 0.96. The strength of the specimen degraded slightly (< 4%) with the increase of the number of cycles at the same displacement amplitude. Therefore, the effect of equal strength substitution of stirrups on the strength degradation coefficient was not obvious.

4.6 Effect of Equal Volume Substitution of Stirrups

Fig. 25 gives the normalized skeleton curves of specimens in group V. The effect of equal volume substitution of stirrups was mainly reflected in the load drop section.

When the maximum load point was reached, the ratio of the maximum load to the yield load of the specimen with HTRB630 stirrups was higher. In the descending section of the load, the load drop rate of the specimen with HTRB630 stirrups was significantly smaller than that of the specimen with HRB400 stirrups.

The lateral strength and displacement ductility coefficient of specimens in group V are shown in Table 14. After the equal volume substitution of stirrups, the lateral strength of specimens was slightly decreased. Theoretically, after the HRB400 stirrups were replaced with HTRB630 stirrups, the strength and the ductility of specimens would not decrease significantly. Therefore, there were problems with the experimental data of specimen T60-3. After the equal volume substitution of stirrups, the elastic modulus of common steel bars and high-strength steel bars were not much different, so the passive restraint stresses of stirrups caused by the same

Sun *et al. Int J Concr Struct Mater*   (2022) 16:45

Page 23 of 28

Table 13 Strength degradation coefficient of specimens in control group IV.

Specimen	Δ/Δ_y	λ			Specimen	Δ/Δ_y	λ		
		Cycle 1	Cycle 2	Cycle 3			Cycle 1	Cycle 2	Cycle 3
T45-2 (HRB400)	2.59	1.000	0.984	0.968	T45-5 (HTRB630)	2.14	1.000	0.987	0.985
	3.46	1.000	0.987	0.973		2.86	1.000	0.994	0.991
	4.32	1.000	0.979	–		3.57	1.000	0.991	0.982
						4.29	1.000	0.988	–
T60-1 (HRB400)	2.74	1.000	0.983	0.977	T60-3 (HTRB630)	1.70	1.000	0.992	0.991
	3.65	1.000	0.980	0.972		2.26	1.000	0.987	0.977
	4.57	1.000	0.989	–		2.83	1.000	0.988	–

Fig. 25 Normalized skeleton curves of specimens in group V.

lateral deformation of concrete were not much different. For the case that the stirrups still did not yield when the specimen was damaged, the high-strength stirrup provided greater strength reserve and redundancy. For the case that the stirrup was close to yield before the failure of specimens, the high-strength stirrups could give full play to the characteristics of high-strength and provide greater lateral restraint stress to slow down the decline of the lateral strength of specimens. The test results of specimen T45-5 supported the theoretical analysis, but the results of specimen T60-3 did not meet the theoretical analysis. Whether it was caused by the quality of the specimen production or another reason needs further testing and comparison.

Fig. 26a gives the cumulative hysteretic energy coefficient E_N curves of specimens in group V. In the initial stage of displacement loading, equal volume substitution of stirrups had little effect on the cumulative dissipation of specimens. After the displacement is increased to $2.0\Delta_y$, the accumulated energy dissipation capacity of specimens with high-strength stirrups was stronger than that of the specimen with common stirrups at the same displacement ductility, and the difference between the two increased as the loading displacement increased.

Fig. 26b gives the average loop stiffness K curves of specimens in group V. The stiffness of the specimen was reduced to a certain extent after equal volume substitution of stirrups. At the same displacement ductility, the stiffness of specimens with high-strength stirrups was significantly lower than that of specimens with common stirrups. The stiffness deterioration rate of specimens was decreased after equal volume substitution of stirrups.

Table 15 shows the strength degradation coefficients of specimens in control group V. The strength degradation coefficient of each specimen was greater than 0.96. The strength of the specimen degraded slightly (< 4%) with the increase of the number of cycles at the same displacement amplitude. Therefore, the effect of equal volume substitution of stirrups on the strength degradation coefficient was not obvious.

Table 14 Lateral strength and displacement ductility of specimens in group V.

Specimen	Concrete	n	A_s	A_{sv}	P_y (kN)	Δ_y (mm)	P_{max} (kN)	Δ_{max} (mm)	P_u (kN)	Δ_u (mm)	μ
T45-2	C45	0.25	4D14	C8@100(2)	75.42	7.00	86.16	16.58	73.23	27.66	3.97
T45-5	C45	0.25	4D14	D8@100(2)	67.19	8.39	78.87	17.44	67.04	37.19	4.51
T60-1	C60	0.25	4D14	C8@100(2)	85.10	5.86	97.94	13.30	83.25	25.92	4.44
T60-3	C60	0.25	4D14	D8@100(2)	79.81	9.42	93.25	16.88	79.26	25.27	2.68

(a) E_N (b) K

Fig. 26 Seismic performance of specimens in group V.
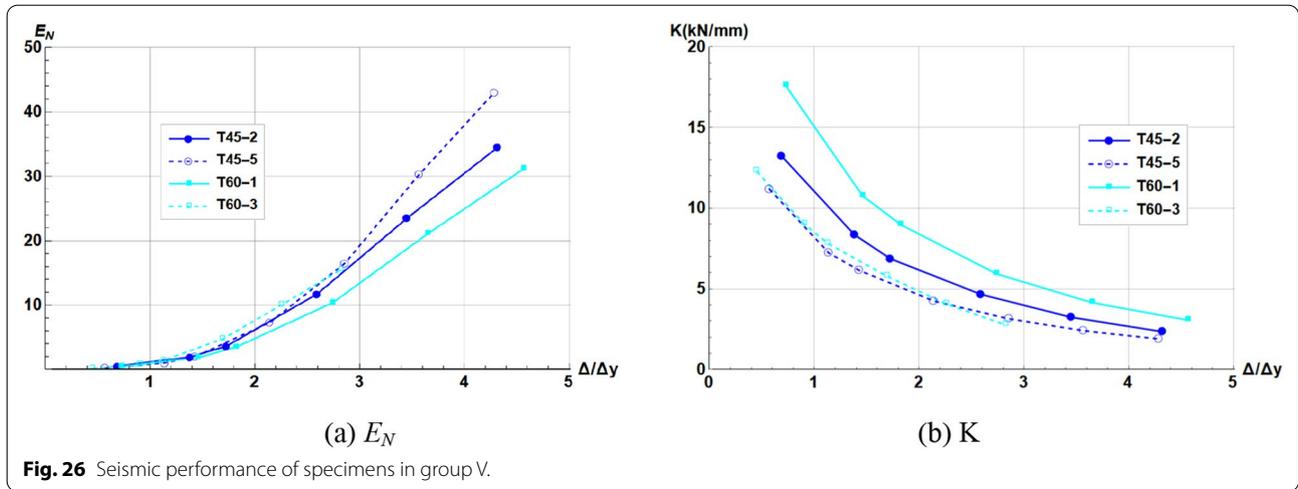
Table 15 Strength degradation coefficient of specimens in control group V.

Specimen	Δ/Δ_y	λ			Specimen	Δ/Δ_y	λ		
		Cycle 1	Cycle 2	Cycle 3			Cycle 1	Cycle 2	Cycle 3
T45-2 (HRB400)	2.59	1.000	0.984	0.968	T45-5 (HTRB630)	2.14	1.000	0.987	0.985
	3.46	1.000	0.987	0.973		2.86	1.000	0.994	0.991
	4.32	1.000	0.979	–		3.57	1.000	0.991	0.982
						4.29	1.000	0.988	–
T60-1 (HRB400)	2.74	1.000	0.983	0.977	T60-3 (HTRB630)	1.70	1.000	0.992	0.991
	3.65	1.000	0.980	0.972		2.26	1.000	0.987	0.977
	4.57	1.000	0.989	–		2.83	1.000	0.988	–

4.7 Effect of Equal Strength Substitution of Confined Stirrups

Fig. 27 gives the normalized skeleton curves of specimens in group VI. At about $1.0\Delta_y$, the specimen of high-strength stirrups had obvious secondary strengthening points, and the rate of descending section was slow. In the elastic stage, the stiffness of the specimen with HTRb630 stirrups was also slightly larger than that of the specimen with HRB400 stirrups.

The lateral strength and displacement ductility of specimens in group VI are shown in Table 16. The carrying capacity was slightly improved. The displacement ductility coefficient of specimen T60-5 was 18.61% larger than that of specimen T60-4. In Sect. 4.5, the displacement ductility coefficient of specimens with high-strength concrete was decreased significantly after equal strength substitution of stirrups. This difference further illustrated that the effects of equal strength substitution of stirrups were based on similar constraints. Only under the premise of ensuring confining effect of stirrups, can the

Fig. 27 Normalized skeleton curves of specimens in group VI.
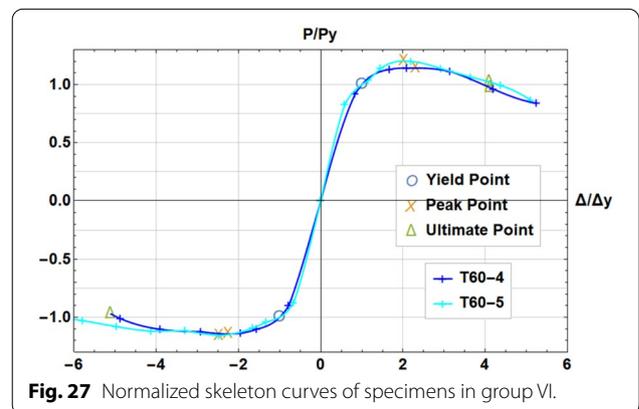
purpose of saving steel bars be avoided without affecting the seismic performance of specimens.

Fig. 28a gives the cumulative hysteretic energy coefficient E_N curves specimens in group VI. With the increase of the displacement, the cumulative energy dissipation

Sun *et al. Int J Concr Struct Mater*   (2022) 16:45

Page 25 of 28

Table 16 Lateral strength and displacement ductility of specimens in group VI.

Specimen	Concrete	n	A_s	A_{sv}	P_y (kN)	Δ_y (mm)	P_{max} (kN)	Δ_{max} (mm)	P_u (kN)	Δ_u (mm)	μ
T60-4	C60	0.25	4D14	D 8@50(2)	78.40	6.22	89.64	14.19	76.20	28.85	4.62
T60-5	C60	0.25	4D14	D 8@75(2)	80.50	6.94	94.83	15.51	80.60	37.44	5.48

(a) E_N

(b) K

(c) Rebar strain
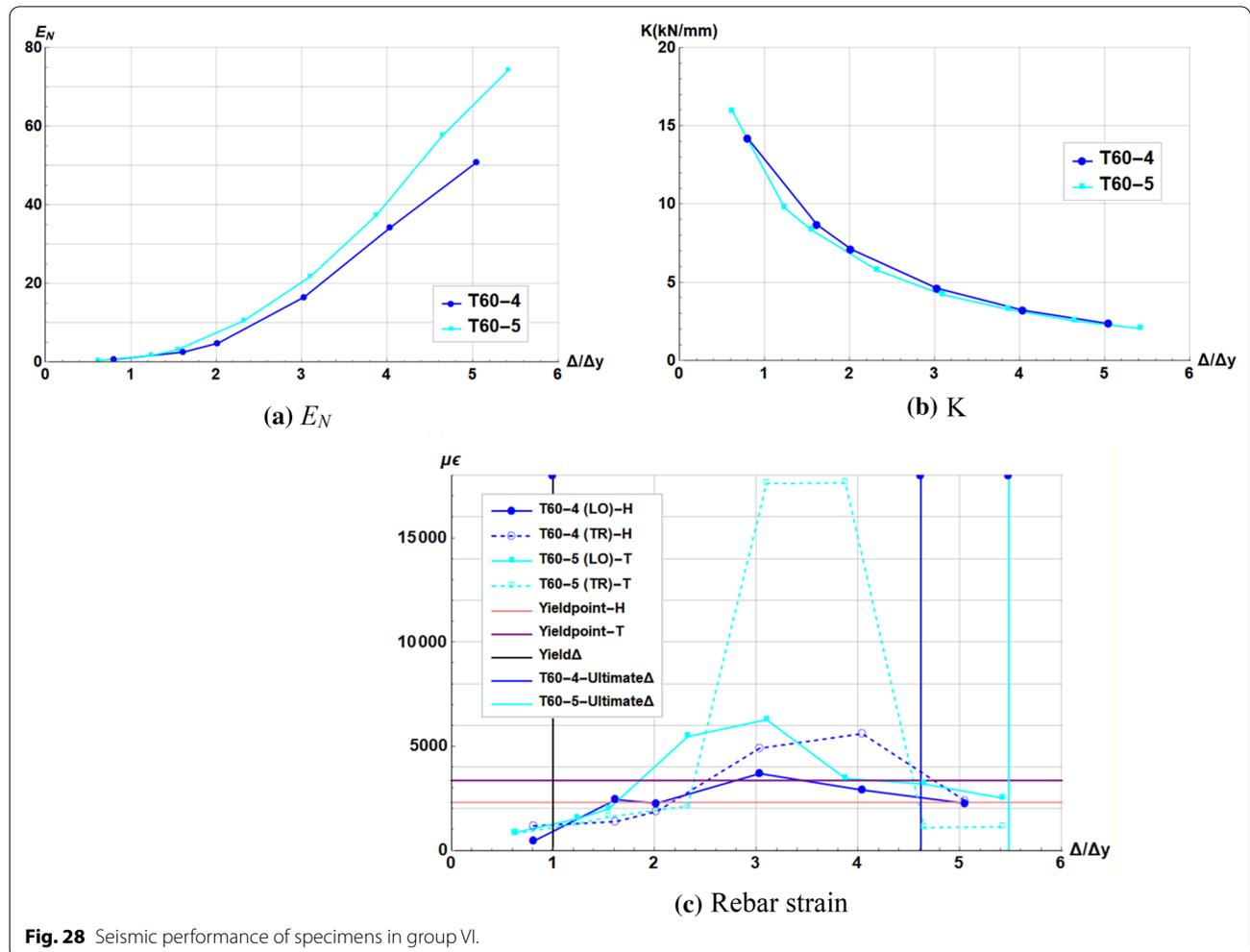
Fig. 28 Seismic performance of specimens in group VI.

capacity of the specimen with high-strength confined stirrups was significantly improved than that of the specimen with common constrained stirrups. The total accumulated energy dissipation of specimens with high-strength confined stirrups was increased significantly by 46.09%.

Fig. 28b gives the average loop stiffness K curves of specimens in group VI. The trend of the loop stiffness degradation curve of the two specimens was exactly the same. Equal strength of confined stirrups would not affect the stiffness of specimens.

Fig. 28c shows the rebar strain envelop curves of specimens in group VI. When the yield displacement was reached, the strain of the longitudinal steel bars of the two specimens did not reach the yield. When the specimens were damaged, the longitudinal reinforcements and stirrups of the two specimens had yielded. The rebar strain of the specimen with confined stirrups was significantly larger than that of the first 11 specimens, which indicated that confined stirrups could not only enhance the ductility of specimens, but also make full use of the

Sun *et al. Int J Concr Struct Mater*   (2022) 16:45

Page 26 of 28

Table 17 Strength degradation coefficient of specimens in control group VI.

Specimen	Δ/Δ_y	λ			Specimen	Δ/Δ_y	λ		
		Cycle 1	Cycle 2	Cycle 3			Cycle 1	Cycle 2	Cycle 3
T60-4 (HRB400)	3.03	1.000	0.992	0.966	T60-5 (HTRB630)	2.32	1.000	0.974	0.973
	4.04	1.000	0.980	0.970		3.10	1.000	1.001	0.983
	5.05	1.000	0.997	–		3.87	1.000	0.994	0.987
						4.65	1.000	0.957	0.960
						5.42	1.000	0.985	-

strength of high-strength longitudinal reinforcements and high-strength stirrups.

Table 17 shows the strength degradation coefficients of specimens in control group VI. The cyclic strength degradation of specimen T60-5 at displacement ductility of 4.65 was slightly faster, the strength degradation of other cycles was relatively slight. The strength degradation coefficient of each specimen was greater than 0.95. The strength of the specimen degraded slightly (< 5%) with the increase of the number of cycles at the same displacement amplitude. Therefore, the effect of equal strength substitution of confined stirrups on the strength degradation coefficient was not obvious.

5 Conclusions and suggestions

The pseudo-static test of 10 concrete columns reinforced with HTRB630 high-strength steel bars and 3 concrete columns reinforced with HRB400 was carried out. The failure mode of each specimen was bending failure. The following conclusions and suggestions could be drawn:

(1) Increasing the axial load ratio was not good for the seismic performance of specimens. After the axial load ratio was increased from 0.1 to 0.25, the lateral strength, energy dissipation capacity and stiffness of specimens were significantly improved, but the ductility and total energy dissipation was greatly decreased, and the rate of stiffness degradation was also greatly accelerated. The effect of the axial load ratio on the strength degradation coefficient was not obvious. The seismic performance of the specimen could be improved by reducing the axial load ratio.

(2) The seismic performance of specimens was decreased with the increase of concrete grade. After the concrete grade was increased from C45 to C60, the hysteresis curve was significant pinch, the lateral strength and stiffness decreased rapidly, and the energy dissipation performance also decreased significantly. The effect of concrete grade on the strength degradation coefficient was not obvious. It was recommended to use C60 concrete or higher-strength materials with HTBR630 steel bars.

(3) After equal strength substitution of high-strength longitudinal reinforcements, the lateral strength of the concrete column specimen with HTRB630 reinforcements was slightly increased, the stiffness degradation was more gradual, and the ductility and energy dissipation capacity were reduced, the strength was slightly degraded, but still met the requirements of the code for seismic design of buildings   (GB 50011-2010) (MOHURD, 2016), which could achieve the purpose of saving steel.

(4) After equal strength substitution of HTRB630 stirrups, the seismic performance of specimens was related to the decrease in the confined efficiency of stirrups. Under the premise that the confining effect of stirrups was limited, equal strength substitution of HTRB630 stirrups can achieve good seismic performance while saving steel bars.

(5) After equal volume substitution of high-strength stirrups, although the lateral strength and stiffness were decreased, the ductility, energy dissipation capacity and total energy dissipation of specimens were improved, and the rate of stiffness degradation was slowed down, the strength was slightly degraded.

(6) After equal strength substitution of HTRB630 confined stirrups, the displacement ductility and energy dissipation capacity of high-strength concretes under the large axial compression was improved effectively, the strength was slightly degraded. Compared with the HRB400 steel bars, HTRB630 high-strength steel bars had a better confining effect.

(7) With the increase of longitudinal reinforcement ratio, the lateral strength of HTRB630 high-strength stirrup columns increases, but the lateral strength decreased rapidly after the peak value. Therefore, it was not appropriate to increase the lateral strength by simply increasing the reinforcement ratio of

Sun *et al. Int J Concr Struct Mater*   (2022) 16:45

Page 27 of 28

longitudinal reinforcement. It was recommended to combine the reinforcement ratio of longitudinal reinforcement with composite stirrups to form high-strength and high-deformation stirrups to constrain the concrete columns.

(8) Considering factors, such as safety and applicability, it was recommended to use HTRB630 high-strength stirrups with small spacing in practical projects to confine high-strength concrete columns. The confining effect of the form of stirrups on concrete will be studied in the future.

Authors' Information
Chuanzhi Sun is an Associate Professor of School of Civil Engineering and Architecture at Suqian College;
Mei-Ling Zhuang is an Associate Professor of School of Transportation and Civil Engineering at Nantong University; and a visitor of School of Civil, Environmental & Mining Engineering at The University of Adelaide;
Bo Dong is a Postgraduate student and also works in Jiangsu Province Architectural D&R Institute Ltd., Nanjing, Corresponding author.
Correspondence to Mei_Ling Zhuang.

Availability of data and materials
The data and materials used to support the findings of this study are available from the corresponding author upon request.

Declarations

Ethics approval and consent to participate
Not applicable.

Informed consent
Informed consent was obtained from all individual participants included in this study.

Consent for publication
All the authors agree that the article will be published after acceptance.

Competing interests
The authors declare that they have no competing interests.

Author details
[1]School of Civil Engineering and Architecture, Suqian College, Jiangsu Province 223800 Suqian, China. [2]School of Transportation and Civil Engineering, Nantong University, Jiangsu Province 226019 Nantong, China. [3]School of Civil, Environmental & Mining Engineering, The University of Adelaide, Adelaide 5005, Australia. [4]Jiangsu Province Architectural, D&R Institute Ltd, Jiangsu Province 210029 Nanjing, China.

References
Bayrak, O., & Sheikh, S. A. (1997). High-strength concrete columns under simulated earthquake loading. *ACI Structural Journal, 94*(6), 708–722.

Budek, A. M., Pristley, M., & Lee, C. O. (2002). Seismic design of columns with high-strength wire and strand as spiral reinforcement. *ACI Structural Journal, 99*(5), 660–670.

Lai, B. L., Richard, L. J. Y., & Xiong, M. X. (2019). Experimental study on high strength concrete encased steel composite short columns. *Construction and Building Materials, 228*, 116640.

Li, Z. B., Yu, C. Y., Xie, Y. P., et al. (2019). Size effect on seismic performance of high-strength reinforced concrete columns subjected to monotonic and cyclic loading. *Engineering Structures, 183*, 206–219.

Liu, W. F., Wang, L. Q., Gao, Y. Q., et al. (2014). Experimental study on seismic behavior of high-strength reinforced concrete frame. *China Civil Engineering, 11*, 64–74.

Muguruma, H., & Watanabe, F. (1990). Ductility improvement of high-strength concrete columns with lateral confinement. *Special Publication, 121*, 47–60.

Ousalem, H., Takatsu, H., Ishikawa, Y., et al. (2009). Use of high-strength bars for the seismic performance of high-strength concrete columns. *Journal of Advanced Concrete Technology, 7*(1), 123–134.

Park, R. (1989). Valuation of ductility of structures and structural assemblages from laboratory testing. *Bulletin of the New Zealand National Society for Earthquake Engineering, 22*(3), 155–166.

Rautenberg, J. M., Pujol, S., Tavallali, H., et al. (2012). Reconsidering the use of high-strength reinforcement in concrete columns. *Steel Construction, 37*(4), 135–142.

Su, J. S., Wang, J. J., Wang, W. B., et al. (2014). Comparative experimental research on seismic performance of rectangular concrete columns reinforced with high strength steel. *Journal of Building Structures, 35*(11), 20–27.

Sugano, S., Nagashima, T., Kimura, H., et al. (1990). Experimental studies on seismic behavior of reinforced concrete Members of High-strength Concrete. *Special Publication, 121*, 61–88.

Sun, C. Z., Miao, C. Q., Li, A. Q., et al. (2021). Experimental study on low cycle fatigue properties of 630MPa high strength steel bar. *Journal of Building Structures, 42*(4), 194–202.

Wang, Q. F., Zheng, J. K., & Zhou, B. (2013). Study on seismic behavior of HRBF500 RC column based on hysteretic energy. *China Civil Engineering, 46*(11), 22–28.

Zhang, J. X., Li, Y. Y., & Rong, X. (2015). Study of bearing capacity and duitility behavior of RC bridge piers arranged with HRB500 steel bars. *Bridge Construction, 45*(3), 58–62.

ACI Committee 318. Building code requirements for structural concrete (ACI 318-08) and commentary," American Concrete Institute, Farmington Hills, Michigan, USA, 2008.

Aoyama H, Murota T, Hiraishi H, Bessho, S. (1992). Development of advanced reinforced concrete buildings with high-strength and high-quality materials. In: Proceedings of the tenth world conference on earthquake engineering (pp. 3365–3370).

BS. Eurocode 2: Design of Concrete Structures (2004). Part 1. General rules and rules for buildings. 2004. British Standards Institution, Brussels, Belgium

Jiangsu Tianshun Metal Materials Group Co., Ltd. and School of Civil Engineering in Southeast University (2012). Jiang Su JG/T 054–2012 Technical

Sun *et al. Int J Concr Struct Mater*   (2022) 16:45

Page 28 of 28

Specification for Heat-treated Ribbed High-strength Reinforced Concrete Structures. Nanjing: Jiangsu Science and Technology Press.

MOHURD (Ministry of Housing and Urban-Rural Development of the People's Republic of China) (2012). Standard for test method of concrete structures (GB/T 50152–2012). Beijing: China Architecture & Building Press.

MOHURD (Ministry of Housing and Urban-Rural Development of the People's Republic of China) (2015). Specification for Seismic Test of Buildings (JGJ/T 101-2015). Beijing: China Architecture & Building Press.

MOHURD (Ministry of Housing and Urban-Rural Development of the People's Republic of China) (2015). Code for design of concrete structures (GB50010-2010). Beijing: China Architecture & Building Press.

MOHURD (Ministry of Housing and Urban-Rural Development of the People's Republic of China) (2016). Code for seismic design of buildings (GB50011-2010). Beijing: China Architecture & Building Press.

National standards of People's Republic of China (2010). Metallic materials-Tensile tests-Part 1: Test methods at room temperature GB/T228.1-2010. Beijing: China Standard Press.

Sun, Z.G., Si, B. J., Wang D. S., Yu, D. H. (2010). Research on confining reinforcement for high-strength concrete columns with high-strength stirrups. Engineering Mechanics 27(10): 182–189, 213.

T63 Heat Treatment Technical Specification for Ribbed High Strength Reinforced Concrete Structure: Q/321182 KBC001-2016 (2016). Engineering Construction Standard Station of Jiangsu Province.

Wang, J. J., Su, J. S., Wang, W. B., Dong, Z. F., Liu, B. (2015). Experiment on seismic performance of circular concrete columns reinforced with HRB500, HRB600 Steel. China Journal of Highway and Transport 28(5): 93–100,107.

Publisher's Note

Springer Nature remains neutral with regard to jurisdictional claims in published maps and institutional affiliations.